Avila G, Lee E, Perez CF, Allen PD, Dirksen RT. FKBP12 binding to *RYR1* modulates excitation-contraction coupling in mouse skeletal myotubes. J Biol Chem 2003b; 278: 22600–8.

Balshaw D, Gao L, Meissner G. Luminal loop of the ryanodine receptor: a pore-forming segment? Proc Natl Acad Sci USA 1999; 96: 3345–7.

Davis MR, Haan E, Jungbluth H, Sewry C, North K, Muntoni F, et al. Principal mutation hotspot for central core disease and related myopathies in the C-terminal transmembrane region of the *RYR1* gene. Neuromuscul Disord 2003; 13: 151–7.

Ferreiro A, Monnier N, Romero NB, Leroy JP, Bonnemann C, Haenggeli CA, et al. A recessive form of central core disease, transiently presenting as multi-minicore disease, is associated with a homozygous mutation in the ryanodine receptor type 1 gene. Ann Neurol 2002; 51: 750–9.

Fletcher JE, Tripolitis L, Hubert M, Vita GM, Levitt RC, Rosenberg H. Genotype and phenotype relationships for mutations in the ryanodine receptor in patients referred for diagnosis of malignant hyperthermia. Br J Anaesth 1995; 75: 307–10.

Ibarra M CA, Ichihara Y, Hikita M, Yoshida K, Junji S, Machara Y, et al. Effect of bupivacaine enantiomers on Ca^{2+} release from sarcoplasmic reticulum in skeletal muscle. Eur J Pharmacol 2005; 512: 77–85.

Ibarra M CA, Wu S, Murayama K, Minami N, Ichihara Y, Kikuchi H, et al. Malignant hyperthermia in Japan: mutation screening of the entire ryanodine receptor type 1 gene coding region by direct sequencing. Anesthesiology 2006. In press.

Jungbluth H, Muller CR, Halliger-Keller B, Brockington M, Brown SC, Feng L, et al. Autosomal recessive inheritance of *RYR1* mutations in a congenital myopathy with cores. Neurology 2002; 59: 284–7.

Leong P, MacLennan DH. The cytoplasmic loops between domains II and III and domains III and IV in the skeletal muscle dihydropyridine receptor bind to a contiguous site in the skeletal muscle ryanodine receptor. J Biol Chem 1998; 273: 29958–64.

Lorenzon NM, Beam KG. Calcium channelopathies. Kidney Int 2000; 57: 794–802.

Lyfenko AD, Goonasekera SA, Dirksen RT. Dynamic alterations in myoplasmic Ca^{2+} in malignant hyperthermia and central core disease. Biochem Biophys Res Commun 2004; 322: 1256–66.

Lynch PJ, Tong J, Lehane M, Mallet A, Giblin L, Heffron JJ, et al. A mutation in the transmembrane/luminal domain of the ryanodine receptor is associated with abnormal Ca^{2+} release channel function and severe central core disease. Proc Natl Acad Sci USA 1999; 96: 4164–9.

Magee KR, Shy GM. A new congenital non-progressive myopathy. Brain 1956; 79: 610–21.

Manning BM, Quane KA, Ording H, Urwyler A, Tegazzin V, Lehane M, et al. Identification of novel mutations in the ryanodine-receptor gene (*RYR1*) in malignant hyperthermia: genotype–phenotype correlation. Am J Hum Genet 1998; 62: 599–609.

Manzur AY, Sewry CA, Ziprin J, Dubowitz V, Muntoni F. A severe clinical and pathological variant of central core disease with possible autosomal recessive inheritance. Neuromuscul Disord 1998; 8: 467–73.

Mathews KD, Moore SA. Multiminicore myopathy, central core disease, malignant hyperthermia susceptibility, and RYR1 mutations: one disease with many faces? Arch Neurol 2004; 61: 27–9.

McCarthy TV, Quane KA, Lynch PJ. Ryanodine receptor mutations in malignant hyperthermia and central core disease. Hum Mutat 2000; 15: 410–7.

Monnier N, Romero NB, Lerale J, Nivoche Y, Qi D, MacLennan DH, et al. An autosomal dominant congenital myopathy with cores and rods is associated with a neomutation in the RYR1 gene encoding the skeletal muscle ryanodine receptor. Hum Mol Genet 2000; 9: 2599–608.

Monnier N, Romero NB, Lerale J, Landrieu P, Nivoche Y, Fardeau M, et al. Familial and sporadic forms of central core disease are associated with mutations in the C-terminal domain of the skeletal muscle ryanodine receptor. Hum Mol Genet 2001; 10: 2581–92.

Monnier N, Kozak-Ribbens G, Krivosic-Horber R, Nivoche Y, Qi D, Kraev N, et al. Correlations between genotype and pharmacological, histological, functional, and clinical phenotypes in malignant hyperthermia susceptibility. Hum Mutat 2005; 26: 413–25.

Quane KA, Healy JM, Keating KE, Manning BM, Couch FJ, Palmucci LM, et al. Mutations in the ryanodine receptor gene in central core disease and malignant hyperthermia. Nat Genet 1993; 5: 51–5.

Quinlivan RM, Muller CR, Davis M, Laing NG, Evans GA, Dwyer J, et al. Central core disease: clinical, pathological, and genetic features. Arch Dis Child 2003; 88: 1051–5.

Robinson RL, Brooks C, Brown SL, Ellis FR, Halsall PJ, Quinnell RJ, et al. *RYR1* mutations causing central core disease are associated with more severe malignant hyperthermia in vitro contracture test phenotypes. Hum Mutat 2002; 20: 88–97.

Romero NB, Monnier N, Viollet L, Cortey A, Chevallay M, Leroy JP, et al. Dominant and recessive central core disease associated with *RYR1* mutations and fetal akinesia. Brain 2003; 126: 2341–9.

Sambrook J, Russell DW. Molecular cloning: a laboratory manual. Cold Spring Harbor, NY: Cold Spring Harbor Laboratory Press; 2001.

Sewry CA, Muller C, Davis M, Dwyer JS, Dove J, Evans G, et al. The spectrum of pathology in central core disease. Neuromuscul Disord 2002; 12: 930–8.

Shepherd S, Ellis F, Halsall J, Hopkins P, Robinson R. *RYR1* mutations in UK central core disease patients: more than just the C-terminal transmembrane region of the *RYR1* gene. J Med Genet 2004; 41: e33.

Shuaib A, Paasuke RT, Brownell KW. Central core disease. Clinical features in 13 patients. Medicine (Baltimore) 1987; 66: 389–96.

Stewart SL, Hogan K, Rosenberg H, Fletcher JE. Identification of the Arg1086His mutation in the alpha subunit of the voltage-dependent calcium channel (CACNA1S) in a North American family with malignant hyperthermia. Clin Genet 2001; 59: 178–84.

Tilgen N, Zorzato F, Halliger-Keller B, Muntoni F, Sewry C, Palmucci LM, et al. Identification of four novel mutations in the C-terminal membrane spanning domain of the ryanodine receptor 1: association with central core disease and alteration of calcium homeostasis. Hum Mol Genet 2001; 10: 2879–87.

Tong J, McCarthy TV, MacLennan DH. Measurement of resting cytosolic Ca^{2+} concentrations and Ca^{2+} store size in HEK-293 cells transfected with malignant hyperthermia or central core disease mutant Ca^{2+} release channels. J Biol Chem 1999; 274: 693–702.

Treves S, Anderson AA, Ducreux S, Divet A, Bleunven C, Grasso C, et al. Ryanodine receptor 1 mutations, dysregulation of calcium homeostasis and neuromuscular disorders. Neuromuscul Disord 2005; 15: 577–87.

Vainzof M, Muniz VP, Tsanaclis AM, Silva HC, Rusticci MS. Does the A3333G mutation in the CACNL1A3 gene, detected in malignant hyperthermia, also occur in central core disease? Genet Test 2000; 4: 383–6.

Weiss RG, O'Connell KM, Flucher BE, Allen PD, Grabner M, Dirksen RT. Function analysis of the R1086H malignant hyperthermia mutation in the DHPR reveals an unexpected influence of the III-IV loop on skeletal muscle EC coupling. Am J Physiol Cell Physiol 2004; 287: 1094–102.

Zhang Y, Chen HS, Khanna VK, De Leon S, Phillips MS, Schappert K, et al. A mutation in the human ryanodine receptor gene associated with central core disease. Nat Genet 1993; 5: 46–50.

Zhao M, Li P, Li X, Zhang L, Winkfein RJ, Chen SR. Molecular identification of the ryanodine receptor pore-forming segment. J Biol Chem 1999; 274: 25971–4.

Zorzato F, Yamaguchi N, Xu L, Meissner G, Muller CR, Pouliquin P, et al. Clinical and functional effects of a deletion in a COOH-terminal luminal loop of the skeletal muscle ryanodine receptor. Hum Mol Genet 2003; 12: 379–88.

Human Molecular Genetics, 2007, Vol. 16, No. 2 115–128
doi:10.1093/hmg/ddl446
Advance Access published on December 12, 2006

A *Gne* knockout mouse expressing human V572L mutation develops features similar to distal myopathy with rimmed vacuoles or hereditary inclusion body myopathy

May Christine V. Malicdan, Satoru Noguchi*, Ikuya Nonaka, Yukiko K. Hayashi and Ichizo Nishino

Department of Neuromuscular Research, National Institute of Neuroscience, National Center of Neurology and Psychiatry, 4-1-1 Ogawahigashi-cho, Kodaira, Tokyo 187-8502, Japan

Received October 3, 2006; Revised November 2, 2006; Accepted November 21, 2006

Distal myopathy with rimmed vacuoles (DMRV) or hereditary inclusion myopathy (h-IBM) is an early adult-onset distal myopathy caused by mutations in the UDP-*N*-acetylglucosamine 2-epimerase/*N*-acetylmannosamine kinase (*GNE*) gene which encodes for a bifunctional enzyme involved in sialic acid biosynthesis. It is pathologically characterized by the presence of rimmed vacuoles especially in atrophic fibers, which also occasionally contain congophilic materials that are immunoreactive to β-amyloid, lysosomal proteins, ubiquitin and tau proteins. To elucidate the pathomechanism of this myopathy and to explore the treatment options, we generated a mouse model of DMRV/h-IBM. We knocked out the *Gne* gene in the mouse, but this resulted in embryonic lethality. We therefore generated a transgenic mouse that expressed the human *GNE*V572L mutation, which is the most prevalent among Japanese DMRV patients, and crossed this with $Gne^{(+/-)}$ mouse to obtain $Gne^{(-/-)}$h*GNE*V572L-Tg. Interestingly, these mice exhibit marked hyposialylation in serum, muscle and other organs. Reduction in motor performance in these mice can only be seen from 30 weeks of age. A compelling finding is the development of β-amyloid deposition in myofibers by 32 weeks, which clearly precedes rimmed vacuole formation at 42 weeks. These results show that the $Gne^{(-/-)}$ h*GNE*V572L-Tg mouse mimics the clinical, histopathological and biochemical features of DMRV/h-IBM, making it useful for understanding the pathomechanism of this myopathy and for employing different strategies for therapy. Our findings underscore the notion that hyposialylation plays an important role in the pathomechanism of DMRV/h-IBM.

INTRODUCTION

Distal myopathy with rimmed vacuoles (DMRV) is an autosomal recessive myopathy which was originally reported by Nonaka *et al.*, (1) thus it is also known as Nonaka myopathy. It is the same entity with hereditary inclusion body myopathy (h-IBM), which was initially reported among Iranian Jews (2). DMRV/h-IBM usually starts affecting adults from ages 15 to 40 years with an average onset of 26 years and with an initial symptom of altered gait (1). It is gradually progressive, and patients become wheelchair-bound between 26 and 57 years of age, or about an average of 12 years after the onset of symptoms (3).

DMRV/h-IBM is characterized by preferential involvement of the distal muscles of lower extremities especially the tibialis anterior muscles, with relative sparing of the quadriceps, hence the term 'quadriceps-sparing' rimmed vacuolar myopathy (2). Other muscles are involved as well, especially late in the course of the disease (3). Serum creatine kinase (CK) level is normal or mildly elevated. The characteristic finding on muscle biopsy is the presence of rimmed vacuoles (RVs), which are actually empty spaces surrounded by aggregation of autophagic vacuoles. These RVs occasionally contain congophilic materials that are immunoreactive to various proteins, including amyloid β, phosphorylated tau, ubiquitin and

*To whom correspondence should be addressed. Tel: +81 423461712; Fax: +81 423461742; Email: noguchi@ncnp.go.jp

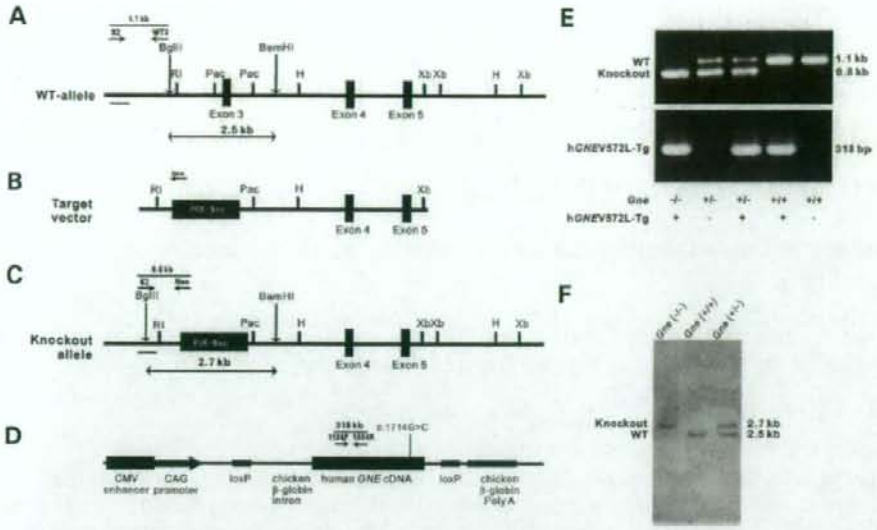

Figure 1. Genomic configuration of the *Gne* gene and targeting vector. Schematic structure of the WT *Gne* gene (**A**), which contains exon 3–5. Positions of restriction enzyme sites are shown. H, *Hin*dIII; Pac, *Pac*I; RI, *Eco*RI; Xb, *Xba*I. A 10.5 kb *Eco*RI–*Xba*I fragment was subcloned to make the targeting vector (**B**). One side of the Neo cassette was inserted 1.4 kb upstream of exon 3, and the other side of which was inserted 124 bp downstream of exon 3. In the knockout allele (**C**), the Neo cassette replaced the 1.4 kb upstream of exon 3, exon 3 and 124 bp downstream of exon 3. We selected homologous recombinants by neomycin resistance. (**D**) Structure of mutated human *GNE*V572L construct. CAG promoter was used to achieve expression in various tissues. (**E**) Genotyping of *Gne* and h*GNE*V572L-Tg mice by PCR. Five genotypes resulting from crossing a $Gne^{(+/-)}$h*GNE*V572L-Tg and $Gne^{(+/-)}$ are shown [from left to right: $Gne^{(-/-)}$ h*GNE*V572L-Tg (+); $Gne^{(+/-)}$h*GNE*V572L-Tg(−); $Gne^{(+/-)}$h*GNE*V572L-Tg(−); $Gne^{(+/+)}$h*GNE*V572L-Tg(+); and $Gne^{(+/+)}$h*GNE*V572L-Tg(−)]. In *Gne* genotyping (upper panel), the 0.8 and 1.1 kb bands represent knockout and WT alleles, respectively [PCR products amplified by primer sets are illustrated in (A) and (C)]. In h*GNE*V572L-Tg genotyping (lower panel), the presence of 318 bp band represents the integration of the h*GNE*V572L transgene. (**F**) Confirmation of *Gne* genotypes by Southern blot analysis. Tail genomic DNA were digested with *Bgl*II and *Bam*HI and analyzed by Southern blot analyses with 5′ probes shown as bars in (A) and (C). The fragments of 2.7 and 2.5 kb represent knockout and WT alleles, respectively.

α-synuclein. Necrotic and regenerating fibers and areas of inflammation are uncommon but can be seen. Ultrastructurally, filamentous inclusions measuring 18–20 nm in diameter are seen in both the cytoplasm and nucleus (3), in addition to the presence of autophagy and various inclusions.

DMRV/h-IBM was mapped to chromosome 9 (4,5), and was shown to be associated with mutations in the *GNE* gene (6,7), which encodes for a bifunctional enzyme that catalyzes the rate-limiting step in sialic acid biosynthesis (8). All patients acquire the disease by autosomal recessive pattern, and have at least one missense mutation in one allele, including the most common mutations V572L and M712T among Japanese and Iranian Jews, respectively. No patient with homozygous null mutation was identified. Genetically confirmed DMRV/h-IBM diseases, initially recognized among Japanese and Iranian Jews (6,9–11), appear to afflict patients with diverse nationalities and cultural backgrounds (12–16).

The mechanism by which mutations in the *GNE* lead to the phenotype in DMRV/h-IBM has remained unclear. We previously demonstrated that mutations in the *GNE* led to the reduction in either the UDP-GlcNAc 2-epimerase or ManNAc kinase activity (17); moreover, we have shown that myotubes from DMRV patients are hyposialylated, and this phenomenon can be corrected by the addition of free sialic acid and/or its precursor. Other groups have shown similar results regarding GNE activity, but in contrast, they suggested that only the cells derived from a patient carrying a homozygous epimerase mutation had a significant reduction in the overall membrane-bound sialic acid (18), and that *GNE* mutations may not contribute to alteration in sialylation in h-IBM myoblasts (19). To address these issues, we developed a mouse model for the disease. In this article, we present the first DMRV/h-IBM mouse model that expressed only the mutated human *GNE* and show that this mouse evidently displays features of DMRV/h-IBM seen in human patients.

RESULTS

Production of $Gne^{(-/-)}$h*GNE*V572L-Tg

In Figure 1, the genomic configuration of the *Gne* gene (A) and the targeting construct (B) are shown. The inserted Neo cassette replaced the 1.4 kb upstream of exon 3, exon 3 and 1.4 kb downstream of exon 3. Only WT and $Gne^{(+/-)}$ mice were generated; no $Gne^{(-/-)}$ mouse was produced (data not shown), in concurrence with a previous report (20). We then proceeded to generate a transgenic mouse (h*GNE*V572L-Tg) that expressed the human mutated *GNE* with V572L, the most common *GNE* mutation in Japan, the structure of which is shown in Figure 1D. Of the resulting litters, nine

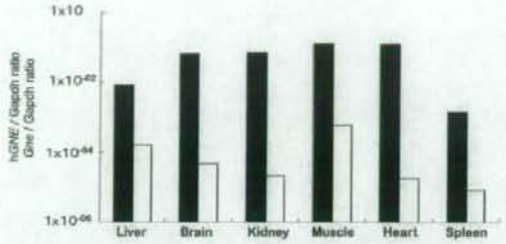

Figure 2. Expression of h*GNE*V572L (closed bars) and endogenous *Gne* (open bars) relative to Gapdh. Log-values were used for computation of ratio. Highest expression of h*GNE*V572L is seen in skeletal and cardiac muscles, followed by heart, kidney, brain, liver and spleen.

mice were found to incorporate the h*GNE*V572L by PCR analysis of genomic DNA isolated from tail snips, but only four lines were able to generate offspring. Using quantitative RT-PCR, we quantified mRNA expression of h*GNE*V572L and endogenous *Gne* in muscle and other organs of these transgenic mice. Transgene expression was highest in the skeletal muscle, followed by heart, kidney, brain, spleen and liver (Fig. 2), while endogenous *Gne* expression was barely detected. We also determined the copy number using quantitative PCR by comparing the amplification of h*GNE*V572L with endogenous *Gne*. We calculated the copy numbers for lines 3, 6, 7 and 9 as 2, 4, 3 and 5, respectively. Consequently, we used this transgenic line 9 for producing the model mouse.

We crossed the h*GNE*V572L transgenic mouse with a $Gne^{(+/-)}$ to obtain a $Gne^{(+/-)}$h*GNE*V572L-Tg. Further, we crossed this $Gne^{(+/-)}$h*GNE*V572L-Tg with a $Gne^{(+/-)}$ to generate our model mouse, a transgenic mouse on a *Gne* knockout background, $Gne^{(-/-)}$h*GNE*V572L-Tg. Analysis of 823 newborn mice from independent heterozygous crosses indicated that the numbers of mice with the five genotypes, $Gne^{(-/-)}$h*GNE*V572L-Tg(+), $Gne^{(+/-)}$h*GNE*V572L-Tg(+), $Gne^{(+/-)}$h*GNE*V572L-Tg(−), $Gne^{(+/+)}$h*GNE*V572L-Tg(+) and $Gne^{(+/+)}$h*GNE*V572L-Tg(−) were 72 (9%), 225 (28%), 193 (24%), 177 (22%) and 136 (17%), respectively, almost approximating the expected ratio of Mendelian inheritance. Mice of the latter four genotypes did not demonstrate unusual phenotype, and thus were considered as control littermates. Images for routine PCR for checking *Gne* genotype and the incorporation of the human *GNE*V572L are shown in Figure 1E, with the corresponding PCR fragments illustrated in A, C and D.

Hyposialylation is evident in the $Gne^{(-/-)}$h*GNE*V572L-Tg

Understandably, mutations in the *GNE* can affect sialylation of glycoconjugates because of the gene's role in sialic acid synthesis. We therefore measured the sialic acid levels in the $Gne^{(-/-)}$h*GNE*V572L-Tg mice using HPLC with fluorometric detection. In wild-type (WT) mice, sialic acid levels are highest in the brain, followed by the liver, spleen and kidney (Fig. 3B, open boxes). In both skeletal and cardiac muscles, sialic acid levels are evidently lower than in other tissues. As we have expected, the total sialic acid in the $Gne^{(-/-)}$h*GNE*V572L-Tg mice is remarkably lower than WT. This hyposialylation is most remarkable in the serum (Fig. 3A). A significant reduction in total sialic acid level is seen in various tissues examined (Fig. 3B, closed boxes). We also measured sialic acid level in the h*GNE*V572L-Tg and noted that sialic acid levels are comparable with WT mice (Fig. 3B, gray boxes), although the transgenic expression was extremely higher than endogenous *GNE*.

$Gne^{(-/-)}$h*GNE*V572L-Tg has lower median of survival than littermate

The $Gne^{(-/-)}$h*GNE*V572L-Tg mice were indistinguishable from their littermates at birth and seemed healthy (Fig. 4A and B). After 30 weeks of age, these mice weighed less than their littermates (Fig. 4). Significant difference in weight is more pronounced and earlier in female $Gne^{(-/-)}$ h*GNE*V572L-Tg (Fig. 4C) mice when compared with male (Fig. 4D). To investigate plausible explanations for this difference in weight, we performed gross inspection of the muscles, and found out that some muscles, especially the gastrocnemius, were atrophic in the $Gne^{(-/-)}$h*GNE*V572L-Tg when compared with control (Fig. 4E and F), and this finding was more remarkable among females (Fig. 4E).

Surprisingly, the median survival rate were lower in the $Gne^{(-/-)}$h*GNE*V572L-Tg as seen in Figure 4B. The cause of death could not be ascertained, but upon necropsy, no external gross abnormalities were seen and the internal organs appeared normal. On pathological examination, five out of 12 (41%) mice that died had RVs in the skeletal muscle; among these five mice, only one was before 40 weeks of age. Twenty five percent had fibrosis and a few RVs in the diaphragm. Thirty-three percent had fibrosis in the cardiac muscles.

$Gne^{(-/-)}$h*GNE*V572l-Tg shows clinical phenotype

Using a tool for assessing general muscle strength, these mice notably performed worse than their littermates (Fig. 5A). Interestingly, significant change in muscle power is noted after 30 weeks of age. We then proceeded to measure serum CK activity in the mice and found out that CK was significantly elevated in the $Gne^{(-/-)}$h*GNE*V572L-Tg mice when compared with their littermates (Fig. 5B), albeit the observation that these values are much lower when compared with muscular dystrophy models like $Large^{myd}$ and $Sgcb^{(-/-)}$ mice (data not shown). Because the appearance of phenotype seemed to be related to age, we measured CK activity according to different age groups. From Figure 5C, we note that elevation of CK activity starts at 30 weeks of age. Using gel electrophoresis, we verified that CK-MM isozyme was primarily increased (data not shown).

$Gne^{(-/-)}$h*GNE*V572l-Tg shows characteristic pathological features of DMRV

We checked if the $Gne^{(-/-)}$h*GNE*V572L-Tg mice showed muscle phenotype not only by the analysis of muscle power

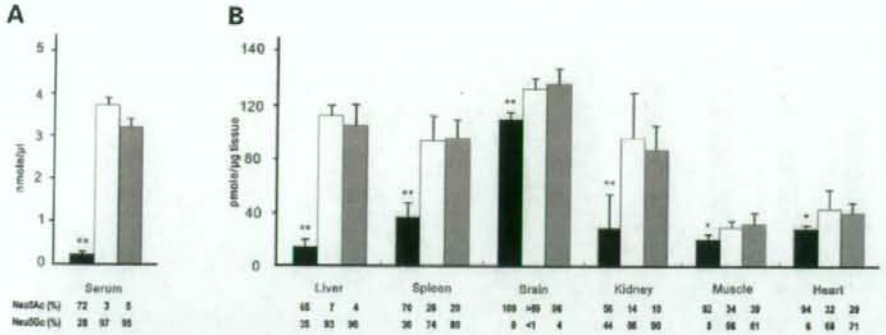

Figure 3. Measurement of total sialic acid in serum (**A**) and tissues (**B**) in *Gne*$^{(-/-)}$hGNEV572L-Tg (closed bars), WT (open bars) and hGNEV572L-Tg (gray bars); bars represent mean total sialic acid level with SD. Breakdown of sialic acid contents according to standards used (Neu5Ac and Neu5Gc) are shown below. Sialic acid levels of WT and hGNEV572L-Tg are comparable. Note the reduction of sialic acid levels in the serum and tissues of the *Gne*$^{(-/-)}$hGNEV572L-Tg mice. Single asterisk, $P < 0.05$; double asterisks, $P < 0.005$.

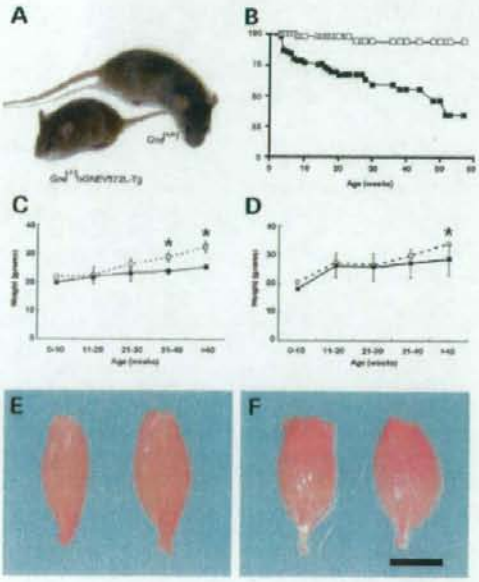

Figure 4. Overall phenotype of the *Gne*$^{(-/-)}$hGNEV572L-Tg mice. (**A**) Picture of WT (up) and *Gne*$^{(-/-)}$hGNEV572L-Tg (down) at 16 weeks of age. (**B**) Survival curve of mice: WT (open squares, $n = 71$ for males and females), *Gne*$^{(-/-)}$hGNEV572L-Tg mice (closed squares, $n = 71$ for males and females). *Gne*$^{(-/-)}$hGNEV572L-Tg mice have significantly reduced life spans when compared with WT mice (log-rank test: $P = 0.001$). (**C**) Growth curves of female: WT (open squares, $n = 10$ per age group), *Gne*$^{(-/-)}$hGNEV572L-Tg mice (closed squares, $n = 10$ per age group) (**D**) Growth curves of male mice: WT (open squares, $n = 10$ per age group), *Gne*$^{(-/-)}$hGNEV572L-Tg (closed squares, $n = 10$ per age group). *Gne*$^{(-/-)}$hGNEV572L-Tg mice have lower body weight after 30 weeks of age, and this is more pronounced in females; asterisk denotes $P < 0.05$, Mann–Whitney U test. Gastrocnemius muscles of female (**E**) and male (**F**) mice: *Gne*$^{(-/-)}$hGNEV572L-Tg (left) and littermate (right). Atrophy is noted on gross inspection of hGNEV572L-Tg gastrocnemius muscles; bar represents 5 mm.

but also by evaluating biopsy samples in five different age groups (10, 20, 30, 40 and 50 weeks). Morphometric analysis of the fibers in different age groups showed that the variation in fiber size becomes more marked with age, preferentially affecting the gastrocnemius and quadriceps muscles (data not shown); for this reason, we used the gastrocnemius muscle in further experiments. We found that at young age, they developed neither clinical nor pathological phenotype, as they were comparable with WT. Figure 6A, D and G shows representative sections from the *Gne*$^{(-/-)}$hGNEV572L-Tg mice per age group. Histopathological analysis revealed almost normal findings in the muscle sections before 30 weeks of age (data not shown). In general, necrotic and regenerating processes are not observed in the young mice, although a few necrotic fibers are observed as they grow older. No endomysial or perimysial inflammation is seen.

Scattered small angular fibers are noted by 30 weeks of age (Fig. 6A), which is not seen in the littermates (Fig. 6B and C). The variation in fiber size becomes more noticeable as the mice grow older. In addition, fibers appear atrophic by 40 weeks of age, in support with the observation that the gastrocnemius muscle is relatively atrophic by gross inspection. Remarkably after 40 weeks, RVs are seen in scattered fibers (arrows in Fig. 6D and G). Occasionally, inclusion bodies are found in the fibers with or without RVs (arrowhead in Fig. 7A and B). Like in humans, these RVs are intensely stained with acid phosphatase, giving the impression that autophagic process is activated (Fig. 7C). We confirmed this by checking the expression of lysosomal-associated proteins (LAMPs) 1 and 2, and LC3 in muscle sections, all of which are upregulated. LAMP-1 is predominantly expressed within the vicinity of RVs (Fig. 7E). LAMP-2, on the other hand, noticeably is also expressed in the subsarcolemmal areas aside from its localization in the area of RVs (Fig. 7F). LC3 immunoreactivity is almost similar to LAMP-2, except that the perinuclear region is also highlighted (Fig. 7G).

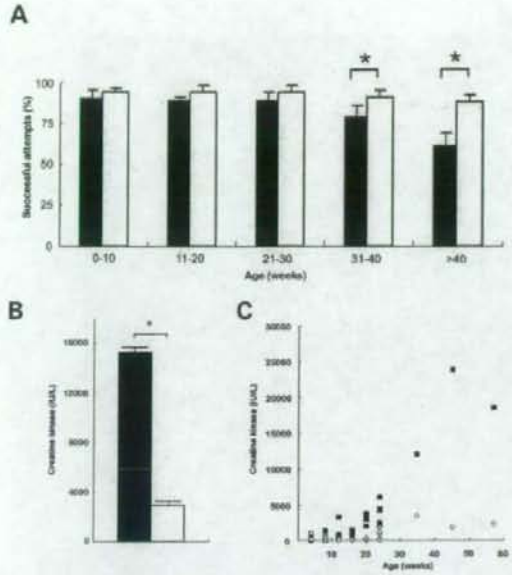

Figure 5. (A) Evaluation of over-all motor strength using rod-climbing test, according to age group. Mean of three trials are shown. $Gne^{(-/-)}$ h*GNE*V572L-Tg mice (closed bars, $n = 10$) perform worse than littermates ($n = 10$). Significant difference is noticeable after 30 weeks of age. Asterisk, $P < 0.05$ (Mann–Whitney U test). (B) Measurement of CK activity. Serum CK is significantly higher in $Gne^{(-/-)}$h*GNE*V572L-Tg mice (closed bars) when compared with littermates (open bars). Asterisk, $P < 0.05$ (Student's t-test, two-tailed). (C) CK activity according to age. CK activity of $Gne^{(-/-)}$ h*GNE*V572L-Tg mice (closed squares) starts to elevate after 30 weeks of age when compared with littermates (open diamonds).

Various proteins are expressed in the $Gne^{(-/-)}$h*GNE*V572L-Tg muscles

One of the defining hallmark features of DMRV/h-IBM is the presence of inclusion bodies that are presumed to have a role in muscle degeneration. These deposits have been shown to be immunoreactive to several proteins. Similar to human cases of DMRV, muscle cross sections obtained from the $Gne^{(-/-)}$ h*GNE*V572L-Tg mice reveal positive Congo red staining (Fig. 7D), which is not observed in the myofibers of control mice (data not shown). Intense, demarcated signals are seen within the area of RVs and more frequently co-localizing with inclusion bodies which are often seen in DMRV/h-IBM. As congophilia denotes deposition of proteins assuming a beta-pleated structure, we used the well-characterized 6E10, Aβ1–42, Aβ1–40 and A11 (amyloid β-oligomer), and β-site amyloid precursor protein cleaving enzyme (BACE2) antibodies to check for intracellular accumulation of amyloid. Amyloid depositions occur within the myofibers, and are seen to be occasionally associated with vacuolated fibers, as ~62% of RVs are positive for amyloid expression (data not shown). These amyloid inclusions are also noted in non-vacuolated fibers, including those which appear normal. Amyloid β precursor protein (AβPP), which is recognized by 6E10 antibody (Fig. 7I) has intense, large, fairly demarcated immunoreactive signals within the RVs, similar to the staining pattern of the fibrillar forms of amyloid β or amyloid β peptides 1–42 and 1–40 (Fig. 7J and K). In good agreement with finding amyloid deposits in the myofibers, BACE2, which purportedly represents β-secretase activity, is upregulated in these myofibers and are seen as granular staining in the cytoplasm and intense immunoreactivity at subsarcolemmal areas (Fig. 7H). Interestingly, the oligomer form of amyloid β, which is recognized by A11, is also expressed in the myofibers; positive signals are seen as aggregates around the RVs which are localized in areas distinct from fibrillar forms of amyloid (Fig. 7L).

We then analyzed skeletal muscles of mice from different age groups to see whether these amyloid accumulations are related to or can be considered as a function of age. We found out that these accumulations start to occur from 32 to 34 weeks of age, a period when virtually no RV is seen in the myofibers, and muscle pathology is characterized mainly by mild variation in fiber size (Fig. 8A and C). Both AβPP (Fig. 8B) and amyloid β 1–42 peptide (Fig. 8D) show positive immunoreactivity within the myofibers.

The microtubule-associated protein tau, a cytoskeletal protein, has been shown to be abnormally phosphorylated and accumulated in DMRV and other muscle disorders (21–23). Similarly, in these mice, these deposits are evident as squiggly inclusions which are occasionally seen in vacuolated fibers (Fig. 7M).

SM-31, an antibody which detects neurofilaments, has been well-characterized in DMRV/h-IBM (21,24). In muscle sections, positive staining is seen within the vicinity of RVs (Fig. 7N); not all RVs, however, show immunoreactivity with this antibody. SM-310, on the other hand, only stains the intramuscular nerve bundles (Fig. 7O).

Because of the accumulation of several proteins in the myofibers, ER stress and the unfolded protein response (UPR) have been implicated in the pathogenesis of DMRV/h-IBM. Using an antibody which recognizes one of the ER chaperones, we show that the UPR activation occurs in the $Gne^{(-/-)}$ h*GNE*V572L-Tg mice. Intracellular Grp-94 immunoreactivity is seen exclusively in vacuolated fibers (Fig. 7P). In the myofibers of the mice, strong reactivity to ubiquitin antibody in vacuolated and non-vacuolated fibers are seen (Fig. 7Q), suggesting that the ubiquitin–proteosome system may as well be involved in the degradation of abnormal protein accumulations in the muscle, and that misfolded proteins are ubiquitinated but not degraded.

Sarcolemmal proteins are also accumulated in DMRV/h-IBM myofibers. Within the vicinity of the RVs, positive α-dystroglycan (Fig. 7R), β-dystroglycan (Fig. 7S) and α-sarcoglycan (Fig. 7T) signals are observed.

In the myofibers of the control mice, no protein depositions were appreciated (data not shown).

Electron microscopic studies show evidence of autophagy and inclusions in the $Gne^{(-/-)}$h*GNE*V572L-Tg muscles

Ultrastructural studies confirm the activation of autophagy in $Gne^{(-/-)}$h*GNE*V572L-Tg muscles (Fig. 9). We obtained samples from a 42-week-old female mouse which had RVs

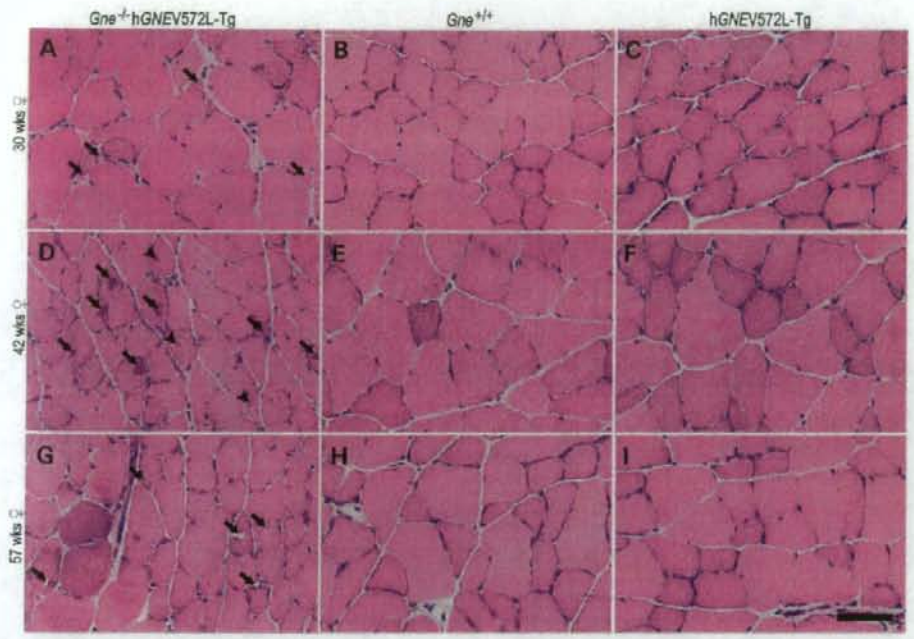

Figure 6. Hematoxylin and eosin sections from $Gne^{-/-}$hGNEV572L-Tg (**A, D, G**), WT (**B, E, H**), hGNEV572L-Tg (**C, F, I**). The hGNEV572L-Tg mice are comparable with WT in all ages. In the $Gne^{-/-}$hGNEV572L-Tg, there is variation in fiber size which becomes more obvious as the mice age. Fibrosis, necrotic or regenerating processes are not noted. Internalized nuclei are noted in scattered fibers. Small angular fibers are noted from around 30 weeks of age (A, arrows). Fibers with RVs (arrows), as well as cytoplasmic inclusions (arrowhead) are observed in scattered fibers from 42 weeks of age (D and G). Bar represents 40 μm.

as seen in light microscopy. In these samples, disorganization of myofibrils was seen in the vicinity of RVs. In about 500 myofibers examined, 10% showed ultrastructural evidence of autophagy. Collections of lysosomal autophagosomes containing undigested intracellular debris were seen, usually enclosed by a limiting membrane (Fig. 9A, arrow). The debris are often composed of light or electron-dense amorphous materials, and appeared like myelin whorls. Multiple small double membrane-bound autophagic vacuoles were often contained within a larger autophagic vesicle (AV), suggesting that autophagy in these myofibers involves a continual process of AV consolidation (Fig. 9A, arrowhead). Multilamellar bodies are also observed (Fig. 9A, double arrows). Probable amyloid deposits are seen as amorphous and granular material (Fig. 9B, magnified from A). Interestingly, ovoid and densely granular deposits, which may also be amyloid-like structures, are noted not only in the areas of autophagy (Fig. 9A, asterisk), but also in areas where myofibrillar architecture is well preserved (Fig. 9C). Occasionally, autophagic vacuoles are seen within the substance of these deposits (Fig. 9C, arrow).

$Gne^{-/-}$hGNEV572L-Tg shows pathological changes in the diaphragm and cardiac muscles

It has been a well-accepted fact that DMRV/h-IBM primarily involved the skeletal muscles, and that respiratory muscles are assumed to be spared as there had been no reports implying the involvement of the respiratory system. Interestingly, in the $Gne^{-/-}$hGNEV572L-Tg mice, we found that even diaphragm muscles are involved, although the findings range from almost normal findings to the presence of marked fibrosis and RVs in the myofibers (Fig. 10A). Likewise, we have observed inclusion bodies which are seen in both vacuolated and non-vacuolated fibers (data not shown).

It is now being recognized that some patients manifest with a variety of cardiac abnormalities, from the seemingly benign right bundle branch block to fatal arrhythmias. This led us to carefully check the status of cardiac muscles in the mice. We found out that few mice (around 20%) develop fibrosis in the cardiac tissue after the age of 30 weeks, and some show marked endomysial fibrosis (Fig. 10B). Moreover, amyloid deposition (Fig. 10C) and, occasionally, RVs (Fig. 10D) are also observed in cardiomyocytes. We also tried to functionally evaluate the heart using 2D echocardiography and electrocardiogram, but we did not observe any abnormality pointing to definite cardiomyopathy or conduction defects (data not shown), although we only tested a limited number of mice.

DISCUSSION

Sialylation of oligosaccharide chains is a common and physiologically important event, and sialic acids are probably the

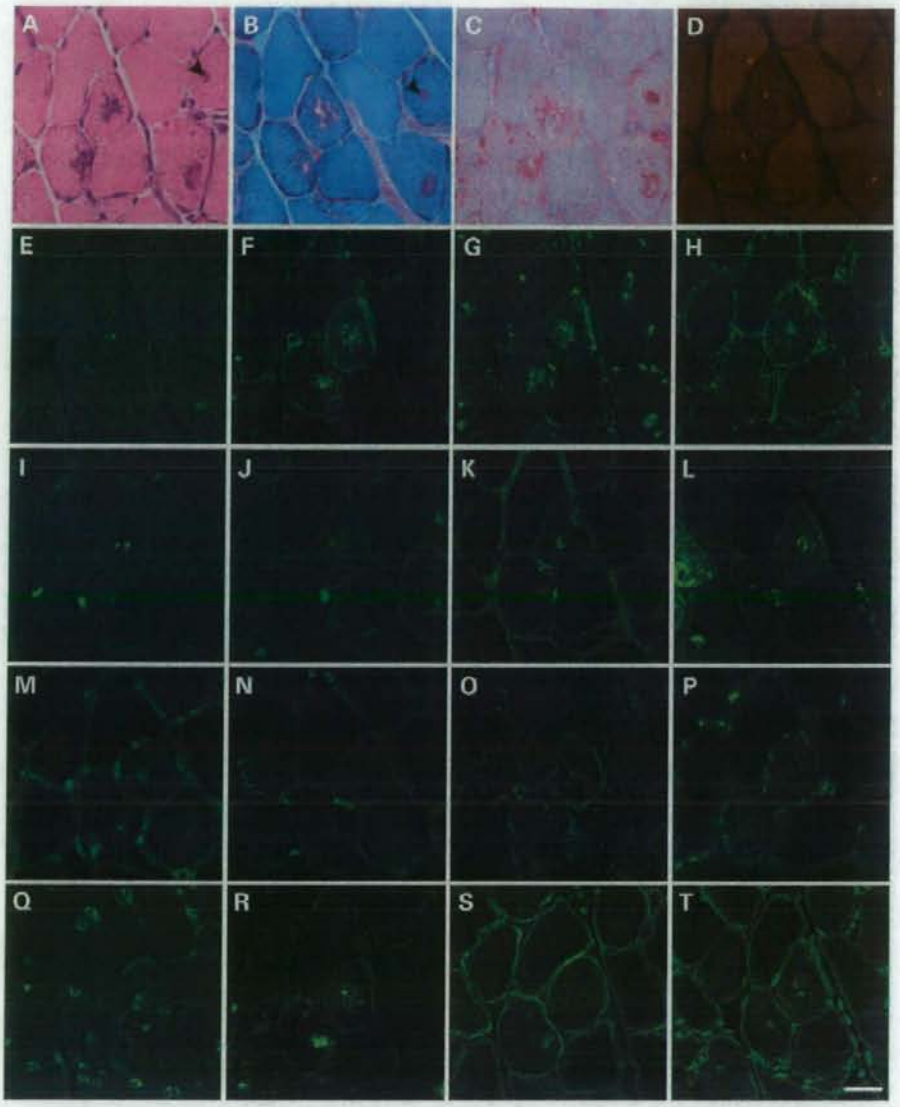

Figure 7. Serial sections taken from a 42-week-old female *Gne*$^{-/-}$;h*GNEV*572L-Tg mouse. (**A**) Hematoxylin and eosin sections show fibers with RVs and cytoplasmic inclusions. (**B**) In modified Gomori trichrome, vacuoles are rimmed by eosinophilic granules. (**C**) Acid phosphatase activity is enhanced around RVs, suggesting upregulation of lysosomal activity in these areas. (**D**) Congo red staining visualized by Texas red filters shows positive staining in fibers with or without RVs, and appear as large, granular deposits. Immunoreactivity to lysosomal proteins confirm the presence of autophagy in fibers with RVs: (**E**) LAMP-1 signals are seen in the areas of RVs; (**F**) LAMP-2 has subsarcolemmal immunoreactivity, in addition to positive staining in RVs; (**G**) LC3 stains the same areas as LAMP-2, in addition to the perinuclear areas. Intracellular deposition of amyloid is seen in vacuolated or non-vacuolated fibers: (**H**) Increased reactivity to BACE2 is seen in the cytoplasm of fibers with RVs and within the vicinity of RVs; (**I**) AβPP expression is intense in area of RVs, seen as discrete deposits; (**J**) amyloid β 1–42 and (**K**) amyloid β 1–40 stainings are likewise seen as discrete deposits within the vicinity of RVs; (**L**) amyloid β-oligomeric antibody signals are noted as aggregates of small granule-like deposits around the RVs. Neurofilament deposition is observed in the myofibers: SM-31 (**M**) immunoreactivity is occasionally noted within the vicinity of RVs, whereas SM-310 (**N**) only stains intramuscular nerve bundles. (**O**) Epitopes of phosphorylated tau are observed in some fibers with RVs. (**P**) Fibers with RVs have intense ubiquitin staining around RVs and granule-like signals in these fibers. (**Q**) Grp94, an endoplastic reticulum luminal stress protein, is upregulated exclusively in vacuolated fibers as large granular deposits within the RVs. Sarcolemmal proteins are deposited within the vicinity of RVs: (**R**) α-dystroglycan; (**S**) β-dystroglycan; and (**T**) α-sarcoglycan. Bar represents 20 μm.

Figure 8. Ultrastructural evidence of autophagy and intracellular inclusions. (**A**) Collections of lysosomal autophagosomes with intracellular debris which are light or electron-dense amorphous materials enclosed by a limiting membrane (arrow). Multilammelar structures are also observed (double arrows). Ovoid and dense deposits which are probably amyloid deposits are likewise seen (asterisk) (**B**) Probable amyloid deposits are seen as amorphous and granular material surrounded by autophagosomes (B, magnified from A). (**C**) Dense, granular deposits which are probably amyloid accumulations are also noted in areas where architecture of myofibrils are generally well preserved; occasionally, autophagic vacuoles are seen within the substance of these deposits (arrow). Bar represents 2 μm.

most biologically important monosaccharide units of glycoconjugates. These negatively charged sugars at the terminal ends of glycoconjugates have very important biological roles in mammalian development, and this is underscored by the embryonic lethality resulting from attempts to knock-out *Gne* in the mice (20), and further supported by the absence of homozygous null mutations in humans. Making a transgenic *GNE* mouse on a *Gne* knockout background thus allowed us to rescue the phenotype in *Gne* knockout. Clearly, the *Gne*$^{(-/-)}$h*GNE*V572L-Tg resembles the phenotype in human DMRV/h-IBM patients.

It is conceivable that a mutation in the *GNE*, a gene responsible for catalyzing the rate-limiting step in sialic acid biosynthesis, can lead to hyposialylation. Most, if not all, of the mutations causing DMRV caused partial reduction of the enzymatic activity of either UDP-GlcNAc 2-epimerase or ManNAc kinase of the GNE (17,19). As we have predicted, our results show that there is a marked reduction in sialic acid level, which can reflect the enzymatic activity of GNE, in the serum and other tissues of the *Gne*$^{(-/-)}$h*GNE*V572L-Tg mice. With regards to the expression of *GNE* in various tissues, it has been shown that expression in the muscle is very low (25). Our results show, on the other hand, that mRNA expression of h*GNE*V572L-Tg is highest in the muscle, and we attribute this to the promoter that we used in the transgene construct. Previously, we have shown that CAG promoter efficiently promotes expression of a gene into adult skeletal muscles (26).

Skeletal muscle is mainly affected in DMRV/h-IBM, although it is reasonable to expect multi-organ involvement because of the ubiquitous expression of *GNE*. In our mice, the skeletal muscle is clearly affected despite the data that

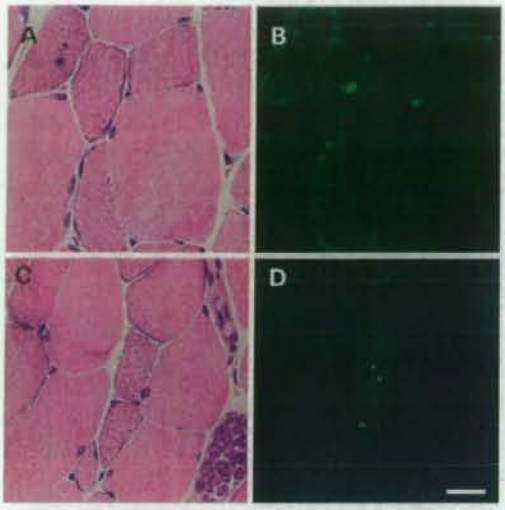

Figure 9. Amyloid deposition precedes RV formation. Sections taken from the gastrocnemius of a 34-week-old female mouse shows variation in fiber size in hematoxylin and eosin sections (**A** and **C**). Note the absence of RVs or cytoplamic inclusions in these fibers. Amyloid depositions are seen as immunofluorescent signals in small fibers (**B**, amyloid β 1–42; **D**, AβPP). Bar represents 20 μm.

hyposialylation is not that remarkable when compared with other organs. Our results suggest that even a slight reduction in sialic acid level can cause symptoms in skeletal muscles; however, the selectivity of skeletal muscle may not be explained by the *Gne* expression levels and sialic acid levels in each organ.

It is notable that some of the $Gne^{(-/-)}$hGNEV572L-Tg mice die sooner than their littermates, but the precise reason for this is not known at present. It is, however, evident that a significant number of the autopsied mice showed pathological findings in the diaphragm and the heart. In humans, there was a report on two siblings with the homozygous V572L mutation who died from arrhythmia (27), but there had been no reports on respiratory involvement among patients.

The onset of symptoms among DMRV patients has been reported to be from the second to the third decade (3), although there were anecdotal reports of earlier onset (28). Interestingly, in the $Gne^{(-/-)}$hGNEV572L-Tg mice, the onset of clinical phenotype is noted around 30 weeks of age, which can be considered to be similar to that in humans, using lifespan and ability to reproduce for points of comparison. It is peculiar that gastrocnemius and quadriceps muscles are preferentially involved in mice, while in humans, the tibialis anterior is remarkably involved while the quadriceps are affected relatively late in the course of the disease. In our recent data on the clinical presentation of DMRV, however, it is clear that the gastrocnemius can be affected more severely in some cases (28).

We tried to check fiber type involvement in these muscles, and found out that both slow and fast fibers are affected in human and mice, in terms of the presence of RVs, but fast type fibers are predominantly involved (data not shown). Sporadic IBM has some pathological similarities with DMRV; recently, it has been shown that the presence of inclusions on routine histochemistry and the pathogenic accumulation of β-amyloid protein occur in fast twitch muscles, both in a transgenic model of IBM and in IBM patients (29), implying that fast type fibers are more vulnerable to pathological changes. Further analysis is needed on this aspect to derive a more conclusive data.

CK levels are reported to be mildly or moderately elevated in patients, although there were isolated cases where the CK activity was above 1000 IU/L (11). CK elevation has always been correlated with the presence of necrotic and regenerating processes in the skeletal muscle, but which are only occasionally found in DMRV/h-IBM. Elevation of serum CK is also seen in the $Gne^{(-/-)}$hGNEV572L-Tg mice, although necrotic and regenerating process is barely detectable. Our data suggest that there might be other mechanisms which trigger CK release into the circulation, aside from myonecrosis. It has not been clarified if CK release into the blood stream may be induced by deglycosylation of membrane proteins, although some studies suggested that removal of sialic acids by neuraminidase treatment may influence sarcolemmal permeability (30). Further tests are clearly needed to shed some insight on the CK elevation in DMRV/h-IBM and $Gne^{(-/-)}$hGNEV572L-Tg mice.

A subject of poignant interest is whether RV formation, one of the hallmarks of DMRV/h-IBM, is the primary event that induces muscle fiber atrophy and loss, notwithstanding the fact that RVs are non-specific and could be seen in a multitude of myopathies. In the $Gne^{(-/-)}$hGNEV572L-Tg mice, weakness is clearly noted before the occurrence of RVs, implying that other factors should be responsible for the earlier onset of weakness. Consistently, we have documented that serum and other tissues are hyposialylated, and this phenomenon is not at all correlated with age, strongly suggesting that hyposialylation may play a role in the development of clinical manifestations exhibited by patients. Previous studies have implicated that sialic acid directly contributes to the negative surface potential of cells, because desialylation of rat skeletal muscle sodium channel leads to reduced sensitivity of these channels to the effects of external calcium (31). This would mean that voltage gating parameters are shifted to the point that channels required a larger depolarization in order to gate, which may suggest that the mechanism of weakness may be due to the reduced excitability of the muscle membrane as a result of sodium channel desialylation.

The hallmarks of DMRV/h-IBM include RVs that are autophagic in nature (32) and cytoplasmic inclusions in vacuolated and non-vacuolated fibers, both of which are seen in muscle sections from the $Gne^{(-/-)}$hGNEV572L-Tg mice. Several proteins have been shown to accumulate in DMRV myofibers (33,34), and most of which have been demonstrated to be mainly associated with amyloid because of the positive reactivity to crystal violet and Congo red, suggesting that they assume the beta-pleated sheet configuration. In general, more than 20 unrelated proteins, including β-amyloid (34), prion, tau (21) and transthyretin, can abnormally unfold and self-aggregate to form beta-pleated sheet amyloid (35). The association of these proteins with DMRV/h-IBM

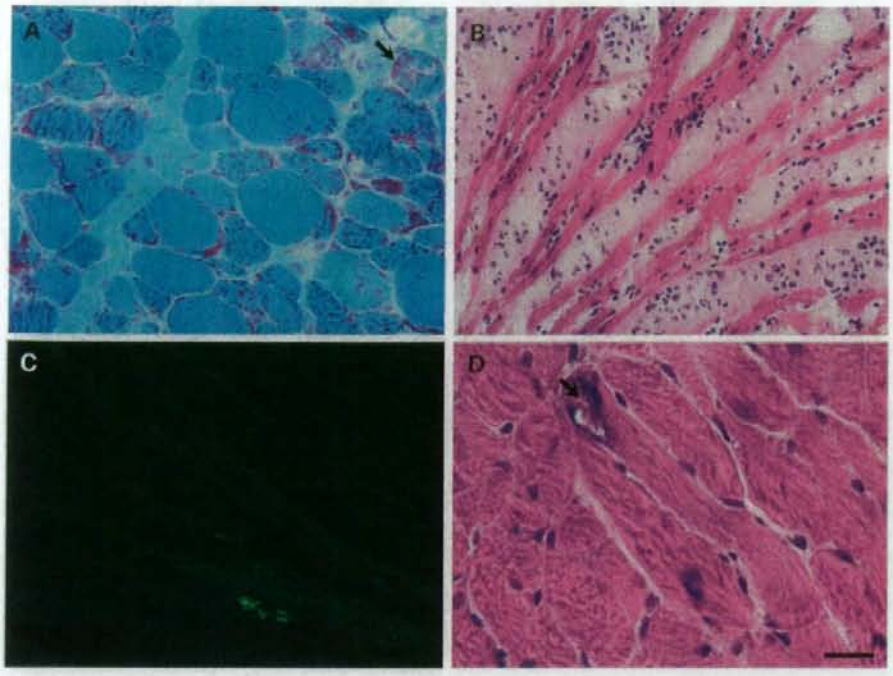

Figure 10. The diaphragm and cardiac muscles are likewise involved in the *Gne*$^{-/-}$h*GNE*V572L-Tg mice. (**A**) Modified Gomori trichrome section of a 48-week-old male *Gne*$^{-/-}$h*GNE*V572L-Tg. Note the presence of endomysial fibrosis and fiber with RV. (**B**) Hematoxylin and eosin sections from a 54-week-old female *Gne*$^{-/-}$h*GNE*V572L-Tg showing marked fibrosis. (**C**) Amyloid deposition (Amyloid β 1–42) is seen in the cardiomyocytes of the same mouse in (B). (**D**) HE section of cardiac muscle from a 42-week-old male *Gne*$^{-/-}$h*GNE*V572L-Tg reveals that RVs are occasionally seen in cardiomyocytes.

pathomechanism has largely been enigmatic up to this time, but unfolding and misfolding of proteins most probably play a role. Previous reports have alluded to the role of sialic acid in proper folding of proteins (35–37). The ultimate fate of aggregated, misfolded glycoproteins is degradation, hence the activation of UPR is expected, which could explain the presence of ubiquitin signals in the myofibers of the *Gne*$^{-/-}$ h*GNE*V572L-Tg mice and upregulation of ubiquitin and proteasome in DMRV/h-IBM myofibers (38).

The implication of amyloid deposition in the formation of RVs in both DMRV/h-IBM and s-IBM (39) is supported by our finding that the occurrence of amyloid inclusions in the myofibers preceded RV formation. Amyloid itself has been shown *in vitro* to block the degradation of ubiquitinated proteins by inhibiting proteasome activity (40), hence its accumulation may not only lead to cytotoxicity, but also may further aggravate protein misfolding. In addition, it has been clarified that overproduction of amyloid can induce tau hyperphosphorylation and decrease its solubility (41). Sialylation and glycosylation of amyloid precursor protein, which contains both *O*- and *N*-glycans, appear to be important for its proteolytic processing, secretion and metabolism (42–45). Interference with the formation of *N*-linked glycans resulted in a decrease in secreted AβPP and an increase in the level of the cellular form of the protein, which has a higher propensity to form amyloid β peptide (42,46). Although amyloid fibrils were the structure previously considered to be cytotoxic, there is current experimental evidence that pre-amyloid oligomeric complexes or aggregates, either diffuse or in a protofibril stage, can be very cytotoxic (47). The presence of dense deposits in areas with relatively preserved myofibrillar architecture on electron microscopy strongly suggest that deposition of amyloid and amyloid-like structures pre-date RV formation.

Because DMRV/h-IBM patients do not present, in general, with symptoms reflecting involvement of the respiratory system, it is assumed that the diaphragm is relatively spared in this myopathy. In the *Gne*$^{-/-}$h*GNE*V572L-Tg mice, it is clear that the diaphragm can be involved, despite the absence of overt respiratory difficulties. The presence of pathological findings in the sacrificed mice, and not only in the ones that died suddenly, may suggest that the presence of RVs *per se*, may not correlate with severity in phenotype, with respect to involvement of diaphragm. A more sensitive method of assessing the respiratory status of these mice, *vis-à-vis* a plain observation, might be helpful in clarifying the extent to which respiratory system is involved. Our results suggest that careful evaluation of respiratory and cardiovascular functions is logical and warranted in human patients.

In the $Gne^{(-/-)}$h*GNE*V572L-Tg mice, we have seen RVs in the cardiac muscles obtained from a couple of mice, clearly supporting the presence of cardiac involvement in DMRV/h-IBM. It has always been reported that DMRV involves primarily skeletal muscles but recently, however, it is being recognized that other organs may likewise be involved. For example, cardiac involvement is not very rare as it is seen in 18% of patients, with a spectrum of manifestations ranging from an incomplete right bundle-branch block to a fatal arrhythmia which led to sudden death (25,26). Sialic acid was shown to be an important component on the surface of heart muscle cells, because its removal reduced the cell surface negative charge by 25% (48) and produced a large increase in cardiac myocyte Ca^{2+}, followed by marked cell contracture (49), emphasizing the importance of negatively charged sialic acid-containing gangliosides in the maintenance of cardiac cell physiological Ca^{2+} permeability. More importantly, it has been demonstrated that in myocardial cells, desialylation of cells by neuraminidase treatment causes aberrant electrical activity (50), and may lead to arrhythmia (51).

In conclusion, we have generated the first mouse model of DMRV/h-IBM, which resembles the clinical, pathological and biochemical features of the disease in humans. The $Gne^{(-/-)}$h*GNE*V572L-Tg mouse is a concrete evidence that mutations in the *GNE* are causative of DMRV/h-IBM. Indeed, these DMRV/h-IBM mice will be a valuable tool to search for further clues in unraveling the pathomechanism of this myopathy. As we have clearly documented in these mice, hyposialylation plays a key role in the pathogenesis of DMRV/h-IBM, and is of paramount importance in considering therapeutic trials.

MATERIALS AND METHODS

Generation of *Gne* knockout mice

The *Gne* knockout mice [$Gne^{(-/-)}$] was produced in inGenious Targeting Laboratory (New York, NY, USA). The 17 kb mouse genomic DNA fragment, containing exons 3–5, was cloned from the mouse 129Sv/Ev lambda genomic library. The Neo cassette that was inserted replaced the 1.4 kb upstream of exon 3, exon 3 and 124 bp downstream of exon 3 (Fig. 1). The resulting targeting vector was linearized by *Not*I, purified and then transfected by electroporation into ES cells. Positive clones after neomycin selection were identified using PCR (primer sequences available upon request).

Generation of h*GNE*V572L-Tg

The cDNA for *GNE* mutant was obtained by reverse transcribed-PCR from skeletal muscle RNA of a DMRV patient with the V572L mutation and cloned into pCR-Blunt vector (Invitrogen, Carlsbad, CA, USA), as described previously (17). Cloned cDNA was sequenced by ABI cycle-sequencing procedures using an ABI 3100 (Applied Biosystems, Foster City, CA, USA). The *Xho*I fragment containing *GNE* mutant cDNA was excised and inserted into pCAGGS vector in which gene expression is driven by a CAG promoter (52). *loxP* sequences were introduced to flank the cDNA insert. *Sal*I fragment was purified and injected into C57BL/6 oocytes and subsequently transplanted into recipient mice. Founders were bred to WT C57BL/6 females to check for germline transmission, which was confirmed by PCR analyses on genomic DNA.

Production of $Gne^{(-/-)}$h*GNE*V572L-Tg

To maintain the same copy number of transgene, stringent measures were taken in generating mice. The h*GNE*V572L-Tg mouse was crossbred to *Gne* heterozygous mouse [$Gne^{(+/-)}$] to create a $Gne^{(+/-)}$ mouse that carried the human *GNE* [$Gne^{(+/-)}$h*GNE*V572L-Tg]. The latter was then mated with a $Gne^{(+/-)}$ mouse, to obtain a mouse that harbors the human V572L mutated *GNE* in a *Gne* knockout background.

For genotyping, DNA was isolated from mouse tails. *Gne* mice genotyping was carried out using PCR analysis on tail genomic DNA with the following primers: Neo, WT3 and S2 (primer sequences available upon request). Further, DNA was digested with *Bam*HI, subjected to Southern blotting and then analyzed by hybridization to a 500 bp probe.

For transgenic mice, the following oligonucleotides were used to amplify a 318 bp segment found specifically in human *GNE*: 1186F, CTTCAAGAGCCACTGCAAA; 1504R, CAATTCCTTCCCGAGGATT.

mRNA expression and determination of copy number

Mouse skeletal muscles, heart, brain, spleen and liver were dissected and rapidly frozen in liquid-nitrogen. Total RNA was extracted from cryostat sections of tissues with TRIzol (Invitrogen) following the manufacturer's protocol. First-strand cDNA was synthesized from RNA by reverse transcription using the Superscript RNase H$^-$ Reverse Transcriptase (Invitrogen) and random hexamers. Gene expression was measured by quantitative real-time PCR in i-Cycler IQ system (Bio-Rad Laboratories, Hercules, CA, USA). Primers (1186F and 1504R) were used to span exon–intron junctions to prevent amplification of genomic DNA. Relative quantification of gene expression was determined by comparison of threshold values as suggested by the manufacturer. All results were normalized with respect to Gapdh expression.

Transgene copy number was determined by the i-Cycler IQ system using the SYBR Green reagent kit according to the manufacturer's instructions. Triplicate samples of tail DNA from transgenic mice of each line were analyzed concurrently against a standard curve of scaled concentrations of an external standard. Primers were designed to amplify the transgene h*GNE*V572L and endogenous *Gne*; twice the ratio of the h*GNE*V572L/*Gne* amplicons was interpreted as copy number.

Sialic acid measurement

The bound sialic acids from the serum and pieces of different tissues were released using 20 mM sulfuric acid hydrolysis for 1 h at 80°C. Free sialic acids were then derivitized with 1, 2-diamino-4, 5-methylenedioxybenzene and analyzed by reverse-phase HPLC fluorescence detection as described previously (53). The eluant was monitored by fluorescence and

Table 1. Antibodies used in the study

Antibody	Manufacturer	Type	Dilution
AβPP (6E10)	Chemicon International Inc., Temecula, CA, USA	Mouse monoclonal	1:1000
Aβ 1–40	Chemicon	Rabbit polyclonal	1:100
Aβ 1–42	Chemicon	Rabbit polyclonal	1:100
Aβ oligomer (A11)	Chemicon	Rabbit polyclonal	1:1000
Human beta site APP cleaving enzyme	Alpha Diagnostic International	Rabbit polyclonal	1:100
Caveolin 3	Transduction Laboratories, Lexington, KY, USA	Rabbit polyclonal	1:400
α-dystroglycan (VIA4-1)	Upstate Cell Signaling Solutions, Lake Placid, NY, USA	Mouse monoclonal	1:100
β-dystroglycan	A gift from Dr Ejiro Ozawa	Rabbit polyclonal	1:200
Grp94 (9G10)	Stressgen Biotechnologies, Calgary, Canada	Rat monoclonal	1:30
LAMP-1 (25)	BD Transduction Laboratories, Lexington, KY, USA	Mouse monoclonal	1:100
LAMP-2A	A gift from Dr Fumitaka Oyama	Rabbit polyclonal	1:100
LC3	A gift from Dr Tamotsu Yoshimori	Rabbit polyclonal	1:200
NCAM (123C3)	Santa Cruz Biotechnology Inc.	Mouse monoclonal	1:100
α-sarcoglycan (Ad1/20A6)	Novocastra Laboratories Ltd.	Mouse monoclonal	1:100
β-sarcoglycan (βSarc/5B1)	Novocastra Laboratories Ltd.	Mouse monoclonal	1:100
polyUbiquitin (FK1)	Biomol International	Mouse monoclonal	1:500
Neurofilament (SM-31)	Sternberg Monoclonals Inc., MD, USA	Mouse monoclonal	1:1000
Neurofilament (SM-310)	Sternberg Monoclonals Inc., MD, USA	Mouse monoclonal	1:1000
tau C	A gift from Dr Fumitaka Oyama	Rabbit polyclonal	1:1000

measured by comparison with Neu5Ac and Neu5Gc standards (from 0.05 nmol/μl to 5 nmol/μl). Total protein from tissues was measured using the Bio-Rad Protein Assay (Bio-Rad Laboratories) according to the manufacturer's protocol.

General assessment for motor strength and fatigability

Whole-animal strength and fatigability were measured according to a test procedure (here referred to as rod-climbing test) previously reported (54). In brief, this test required the mice to pull themselves on top of a suspended rod (3 mm in diameter). The measurement of muscle weakness was based on the mean percentage of passes over 15 trials of the test in a 3-min period. Fatigability was assessed as the average pass rate over time for each group of mice. The test was repeated at least three times after a 2-week period.

Histopathological and histochemical analyses

Fresh specimens from individual skeletal and cardiac muscles were snap-frozen in liquid-nitrogen-cooled isopentane and stored at −80°C until further processing. We stained frozen sections (6 μm) of transversal skeletal and cardiac muscles with a battery of histochemical stains including hematoxylin and eosin, modified Gomori trichrome and acid phosphatase. Sections were analyzed by light microscopy. We performed Congo red staining in 10 μm cryosections following the Putchler's modification, and viewed sections under light microscope and conventional fluorescence microscope using Texas-red filters (39). For immunohistochemical analysis, tissue sections were fixed either in acetone or paraformaldehyde, depending on the primary antibody used, and blocked with 5% normal serum and 2% bovine serum albumin in phosphate-buffered saline. The primary antibodies used are listed in Table 1. We used several antibodies which recognize amyloidβ 6E10, which is a human-specific antibody, but also reacts to murine tissue when the amyloid burden is high, primarily recognizes AβPP (residues 1–16) after α-secretase cleavage. It also recognizes, in addition, C99 fragment and amyloid β peptides (1–40 and 1–42) which have been shown to be prone to aggregation. The anti-oligomeric antibody (A11) is specific to the oligomeric structure of β amyloid peptides. The following secondary antibodies were used appropriately: anti-goat IgG F (ab')-2-fragment, FITC conjugated (EY Laboratories, San Mateo, CA, USA); anti-rabbit IgG (H + L), Alexa Fluor conjugated (Molecular Probes, Eugene, OR, USA); anti-mouse IgG1, FITC conjugated (Sanbio/Monosan, Uden, The Netherlands). Images were collected and analyzed with a laser scanning microscope (Olympus, Tokyo, Japan) with its appropriate software.

Morphometric analysis of fibers

Muscle cross sections were stained with rabbit polyclonal antibody against caveolin-3 followed by a fluorescent secondary antibody. Digital images from fluorescence signals were observed under a confocal microscope and the widest diameter was recorded for 600 or more fibers using Image-J software from the public domain NIH Image program (developed at the U.S. National Institutes of Health and available on the Internet at http://rsb.info.nih.gov/nih-image/). Results were analyzed using Statistics Software for Social Sciences (SPSS for Windows, Rel. 11.0.0. 2001, SPSS Inc., Chicago) software.

Electron microscopy

The muscle specimens were immediately fixed for 2 h in 2.5% cold glutaraldehyde with 0.1 M cacodylate buffer, pH 7.3. After washing in cacodylate buffer, the specimens were post-fixed in 1% osmium tetroxide in the same buffer, dehydrated with graded series of ethanol and embedded in Epon. Semithin sections (0.5 μm) were stained with toluidine blue alkaline. Ultrathin sections were stained with uranyl acetate, citrated and observed with a H-600 electron microscope (Hitachi, Tokyo, Japan) at 75 kV.

Serum CK

Blood samples were obtained either by inferior vena cava aspiration, or careful collection from mouse tail. Total CK activity was measured by a spectrophotometric assay employing a commercial kit (CPK-L Determiner, Kyowa MEDEX, Tokyo, Japan). For confirmation, CK isoforms were electrophoretically analyzed using Titan Gel CK Isozyme kit (Helena Laboratories, Beaumont, TX, USA) following the manufacturer's protocol.

Statistical analysis

Data were entered in SPSS version 11.0 and were analyzed by computation of the frequency and the mean $\pm$ SD and/or percentage. The data were then subjected to a univariate analysis (Fisher's exact test), Student's *t*-test, Wilcoxon paired test, ANOVA or Mann–Whitney *U* test, log-rank test or multiple regression analysis, whichever was appropriate. *P*-values less than 0.05 were considered to be statistically significant.

ACKNOWLEDGEMENTS

The authors thank the following persons for their invaluable support and assistance: Yoko Keira, Genri Kawahara, Mari Okada and Kumiko Murayama. This study is supported by the 'Research on Psychiatric and Neurological Diseases and Mental Health' from Health and Labour Sciences Research Grants; the 'Research on Health Sciences focusing on Drug Innovation' from the Japanese Health Sciences Foundation; the 'Research Grant (16B-2, 17A-10) for Nervous and Mental Disorders' from the Ministry of Health, Labour and Welfare; and the Program for Promotion of Fundamental Studies in Health Sciences of the National Institute of Biomedical Innovation (NIBIO).

Conflict of Interest statement. None declared.

REFERENCES

1. Nonaka, I., Sunohara, N., Ishiura, S. and Satoyoshi, E. (1981) Familial distal myopathy with rimmed vacuole and lamellar (myeloid) body formation. *J. Neurol. Sci.*, **51**, 141–155.
2. Argov, Z. and Yarom, R. (1984) 'Rimmed vacuole myopathy' sparing the quadriceps. A unique disorder in Iranian Jews. *J. Neurol. Sci.*, **64**, 33–43.
3. Nonaka, I., Noguchi, S. and Nishino, I. (2005) Distal myopathy with rimmed vacuoles and hereditary inclusion body myopathy. *Curr. Neurol. Neurosci. Rep.*, **5**, 61–65.
4. Ikeuchi, T., Asaka, T., Saito, M., Tanaka, H., Higuchi, S., Tanaka, K., Saida, K., Uyama, E., Mizusawa, H., Fukuhara, N. *et al.* (1997) Gene locus for autosomal recessive distal myopathy with rimmed vacuoles maps to chromosome 9. *Ann. Neurol.*, **41**, 432–437.
5. Mitrani-Rosenbaum, S., Argov, Z., Blumenfeld, A., Seidman, C.E. and Seidman, J.G. (1996) Hereditary inclusion body myopathy maps to chromosome 9p1-q1. *Hum. Mol. Genet.*, **5**, 159–163.
6. Nishino, I., Noguchi, S., Murayama, K., Driss, A., Sugie, K., Oya, Y., Nagata, T., Chida, K., Takahashi, T., Takusa, Y. *et al.* (2002) Distal myopathy with rimmed vacuoles is allelic to hereditary inclusion body myopathy. *Neurology*, **59**, 1689–1693.
7. Eisenberg, I., Avidan, N., Potikha, T., Hochner, H., Chen, M., Olender, T., Barash, M., Shemesh, M., Sadeh, M., Grabov-Nardini, G. *et al.* (2001) The UDP-*N*-acetylglucosamine 2-epimerase/*N*-acetylmannosamine kinase gene is mutated in recessive hereditary inclusion body myopathy. *Nat. Genet.*, **29**, 83–87.
8. Keppler, T., Hinderlich, S., Langner, J., Schwartz-Albiez, R., Reutter, W. and Pawlita, M. (1999) UDP-GlcNAc 2-epimerase: a regulator of cell surface sialylation. *Science*, **284**, 1372–1376.
9. Eisenberg, I., Grabov-Nardini, G., Hochner, H., Korner, M., Sadeh, M., Bertorini, T., Bushby, K., Castellan, C., Felice, K., Mendell, J. *et al.* (2003) Mutations spectrum of *GNE* in hereditary inclusion body myopathy sparing the quadriceps. *Hum. Mutat.*, **21**, 99.
10. Argov, Z., Eisenberg, I., Grabov-Nardini, G., Sadeh, M., Wirguin, I., Soffer, D. and Mitrani-Rosenbaum, S. (2003) Hereditary inclusion body myopathy: the Middle Eastern genetic cluster. *Neurology*, **60**, 1519–1523.
11. Tomimitsu, H., Shimizu, J., Ishikawa, K., Ohkoshi, N., Kanazawa, I. and Mizusawa, H. (2004) Distal myopathy with rimmed vacuoles (DMRV): new *GNE* mutations and splice variant. *Neurology*, **62**, 1607–1610.
12. Kim, B.J., Ki, C.S., Kim, J.W., Sung, D.H., Choi, Y.C. and Kim, S.H. (2006) Mutation analysis of the *GNE* gene in Korean patients with distal myopathy with rimmed vacuoles. *J. Hum. Genet.*, **51**, 137–140.
13. Ro, L.S., Lee-Chen, G.J., Wu, Y.R., Lee, M., Hsu, P.Y. and Chen, C.M. (2005) Phenotypic variability in a Chinese family with rimmed vacuolar distal myopathy. *J. Neurol. Neurosurg. Psychiatry*, **76**, 752–755.
14. Broccolini, A., Ricci, E., Casssndrini, D., Gliubizzi, C., Bruno, C., Tonoli, E., Silvestri, G., Pescatori, M., Rodolico, C., Sinicropi, S. *et al.* (2004) Novel *GNE* mutations in Italian families with autosomal recessive hereditary inclusion-body myopathy. *Hum. Mutat.*, **23**, 632.
15. Liewluck, T., Pho-Iam, T., Limwongse, C., Thongnoppakhun, W., Boonyapisit, K., Raksadawan, N., Murayama, K., Hayashi, Y.K., Nishino, I. and Sangruchi, T. (2006) Mutation analysis of the *GNE* gene in distal myopathy with rimmed vacuoles (DMRV) patients in Thailand. *Muscle Nerve*, Epub ahead of print.
16. Amouri, R., Driss, A., Murayama, K., Kefi, M., Nishino, I. and Hentati, F. (2005) Allelic heterogeneity of *GNE* gene mutation in two Tunisian families with autosomal recessive inclusion body myopathy. *Neuromuscul. Disord.*, **15**, 361–363.
17. Noguchi, S., Keira, Y., Murayama, K., Ogawa, M., Fujita, M., Kawahara, G., Oya, Y., Imazawa, M., Goto, Y., Hayashi, *et al.* (2004) Reduction of UDP-*N*-acetylglucosamine 2-epimerase/*N*-acetylmannosamine kinase activity and sialylation in distal myopathy with rimmed vacuoles. *J. Biol. Chem.*, **279**, 11402–11407.
18. Salama, I., Hinderlich, S., Shlomai, Z., Eisenberg, I., Krause, S., Yarema, K., Argov, Z., Lochmuller, H., Reutter, W., Dabby, R. *et al.* (2005) No overall hyposialylation in hereditary inclusion body myopathy myoblasts carrying the homozygous M712T GNE mutation. *Biochem. Biophys. Res. Commun.*, **328**, 221–226.
19. Hinderlich, S., Salama, I., Eisenberg, I., Potikha, T., Mantey, L.R., Yarema, K.J., Horstkorte, R., Argov, Z., Sadeh, M., Reutter, W. *et al.* (2004) The homozygous M712T mutation of UDP-*N*-acetylglucosamine 2-epimerase/*N*-acetylmannosamine kinase results in reduced enzyme activities but not in altered overall cellular sialylation in hereditary inclusion body myopathy. *FEBS Lett.*, **566**, 105–109.
20. Schwarzkopf, M., Knobeloch, K.P., Rohde, E., Hinderlich, S., Wiechens, N., Lucka, L., Horak, I., Reutter, W. and Horstkorte, R. (2002) Sialylation is essential for early development in mice. *Proc. Natl Acad. Sci. USA*, **99**, 5267–5270.
21. Mirabella, M., Alvarez, R.B., Bilak, M., Engel, W.K. and Askanas, V. (1996) Difference in expression of phosphorylated tau epitopes between sporadic and hereditary inclusion-body myopathies. *J. Neuropathol. Exp. Neurol.*, **55**, 774–786.
22. Akanas, V. and Engel, W.K. (2006) Inclusion-body myositis: a myodegenerative conformational disorder associated with Abeta, protein misfolding, and proteasome inhibition. *Neurology*, **66** (Suppl. 1), S39–S48.
23. Askanas, V. and Engel, W.K. (2003) Hereditary inclusion myopathies. In Rosenberg, R.N., Prusiner, S.B., DiMauro, S., Barchi, R.L. and Nestler, E.J. (eds), *The Molecular and Genetic Basis of Neurologic and Psychiatric Disease*, 3rd edn. Butterworth–Heinemann, Woburn, MA, USA, pp. 501–509.
24. Akanas, V. and Engel, W.K. (2003) Proposed pathogenic cascade of inclusion-body myositis: importance of amyloid-beta, misfolded proteins, predisposing genes, and aging. *Curr. Opin. Rheumatol.*, **15**, 734–744.
25. Horstkorte, R., Nöhring, S., Wiechens, N., Schwarzkopf, M., Danker, K., Reutter, W. and Lucka, L. (1999) Tissue expression and amino acid sequence of murine UDP-*N*-acetylglucosamine-2-epimerase/*N*-acetylmannosamine kinase. *FEBS J.*, **260**, 923–927.

26. Ishii, A., Hagiwara, Y., Saito, Y., Yamamoto, K., Yuasa, K., Sato, Y., Arahata, K., Shoji, S., Nonaka, I., Saito, I., Nabeshima, Y., Takeda, S. (1999) Effective adenovirus-mediated gene expression in adult murine skeletal muscle. *Muscle Nerve*, **22**, 592–599.
27. Kimpara, T., Imamura, T., Tsuda, T., Sato, K. and Tsuburaya, K. (1993) Distal myopathy with rimmed vacuoles and sudden death—report of two siblings. *Rinsho Shinkeigaku*, **33**, 886–890.
28. Nishino, I., Malicdan, M.C., Murayama, K., Nonaka, I., Hayashi, Y.K. and Noguchi, S. (2005) Molecular pathomechanism of distal myopathy with rimmed vacuoles. *Acta Myol.*, **24**, 80–83.
29. Sugarman, M., Kitazawa, M., Baker, M., Caiozzo, V.J., Querfurth, H.W. and LaFerla, F.M. (2006) Pathogenic accumulation of APP in fast twitch muscle of IBM patients and a transgenic model. *Neurobiol. Aging*, **27**, 423–432.
30. Post, J.A. (1992) Removal of sarcolemmal sialic acid residues results in a loss of sarcolemmal functioning and integrity. *Am. J. Physiol.*, **263**, H147–H152.
31. Bennett, E., Urcan, M.S., Tinkle, S.S., Kozkowski, A. and Levinson, S. (1997) Contribution of sialic acid to the voltage dependence of sodium channel gating: a possible electrostatic mechanism. *J. Gen. Physiol.*, **109**, 327–343.
32. Nishino, I. (2003) Autophagic vacuolar myopathies. *Curr. Neurol. Neurosci. Rep.*, **3**, 64–69.
33. Askanas, V., Alvarez, R.B. and Engel, W.K. (1993) β-Amyloid precursor epitopes in muscle fibers of inclusion body myositis. *Ann. Neurol.*, **34**, 551–560.
34. Askanas, V. and Engel, W.K. (1995) New advances in the understanding of sporadic inclusion-body myositis and hereditary inclusion-body myopathies. *Curr. Opin. Rheumatol.*, **7**, 486–496.
35. Ellis, R. and Pinheiro, T.J.T. (2002) Danger: misfolding proteins. *Nature*, **416**, 483–484.
36. Brooks, S.A., Dwek, M.V. and Schumacher, U. (2002) *Functional and Molecular Glycobiology*. BIOS Scientific Publishers Limited, Oxford, UK.
37. Helenius, A. and Aebi, M. (2004) Roles of *N*-linked glycans in the endoplasmic reticulum. *Annu. Rev. Biochem.*, **73**, 1019–1049.
38. Kumamoto, T., Fujimoto, S., Nagao, S., Masuda, T., Sugihara, R., Ueyama, H. and Tsuda, T. (1998) Proteasomes in distal myopathy with rimmed vacuoles. *Intern. Med.*, **37**, 746–752.
39. Askanas, V., Engel, W.K. and Alvarez, R.B. (1993) Enhanced detection of congo-red-positive amyloid deposits in muscle fibers of inclusion body myositis and brain of Alzheimer's disease using fluorescence technique. *Neurology*, **43**, 1265–1267.
40. Gregori, L., Hainfeld, J.F., Simon, M.N. and Goldbager, D. (1997) Binding of amyloid β protein to the 20S proteasome. *J. Biol. Chem.*, **272**, 58–62.
41. Wang, Y.P., Wang, X.C., Tian, Q., Yang, Y., Zhang, Q., Zhang, J.Y., Zhang, Y.C., Wang, Z.F., Wang, Q., Li, H. *et al.* (2006) Endogenous overproduction of β-amyloid induces tau hyperphosphorylation and decreases the solubility of tau in N2a cells. *J. Neural. Transm.*, Epub ahead of print.
42. McFarlane, I., Georgopoulou, N., Coughlan, C.M., Gillian, A.M. and Breen, K.C. (1999) The role of the protein glycosylation state in the control of cellular transport of the amyloid beta precursor protein. *Neuroscience*, **90**, 15–25.
43. Pahlsson, P. and Spitalnik, S.L. (1996) The role of glycosylation in synthesis and secretion of beta-amyloid precursor protein by Chinese hamster ovary cells. *Arch. Biochem. Biophys.*, **331**, 177–186.
44. Yazaki, M., Tagawa, K., Maruyama, K., Sorimachi, H., Tsuchiya, T., Ishiura, S. and Suzuki, K. (1996) Mutation of potential *N*-linked glycosylation sites in Alzheimer's disease amyloid precursor protein (APP). *Neurosci. Lett.*, **221**, 57–60.
45. Nakagawa, K., Kitazume, S., Oka, R., Maruyama, K., Saido, T.C., Sato, Y., Endo, T. and Hashimoto, Y. (2006) Sialylation enhances the secretion of neurotoxic amyloid-beta peptides. *J. Neurochem.*, **96**, 924–933.
46. Georgopoulou, N., McLaughlin, M., McFarlane, I. and Breen, K.C. (2001) The role of post-translational modification in beta-amyloid precursor protein processing. *Biochem. Soc. Symp.*, **67**, 23–36.
47. Tsai, B., Ye, Y. and Rapoport, T.A. (2002) Retro-translocation of proteins from the endoplasmic reticulum into the cytosol. *Nat. Rev. Mol. Cell Biol.*, **3**, 246–255.
48. Soeiro, M.N., Silva-Filho, F.C. and Meirelles, M.N. (1994) The nature of anionic sites and the endocytic pathway in heart muscle cells. *J. Submicrosc. Cytol. Pathol.*, **26**, 121–130.
49. Marengo, F.D., Wang, S.Y., Wang, B. and Langer, G.A. (1998) Dependence of cardiac cell Ca^{2+} permeability on sialic acid-containing sarcolemmal gangliosides. *J. Mol. Cell Cardiol.*, **30**, 127–137.
50. Woods, W.T., Inamura, K. and James, T.R. (1982) Electrophysiological and electron microscopic correlations concerning the effects of neuraminidase on canine heart cells. *Circ. Res.*, **50**, 228–231.
51. Ufret-Vincenty, C.A., Baro, D.J. and Santana, L.F. (2001) Differential contribution of sialic acid to the function of repolarizing K^+ currents in ventricular myocytes. *Am. J. Physiol. Cell Physiol.*, **281**, C464–C474.
52. Niwa, H., Yamamura, K. and Miyazaki, J. (1991) Efficient selection for high-expression transfectants with a novel eukaryotic vector. *Gene*, **108**, 193–199.
53. Hara, S., Yamaguchi, M., Takemori, Y., Nakamura, M. and Ohkura, Y. (1986) Highly sensitive determination of *N*-acetyl- and *N*-glycolylneuraminic acids in human serum and urine and rat serum by reversed-phase liquid chromatography with fluorescence detection. *J. Chromatogr.*, **377**, 111–119.
54. Keppler, O.T., Hinderlich, S., Langner, J., Schwartz-Albiez, R., Reutter, W. and Pawlita, M. (1999) UDP-GlcNAc 2-epimerase: a regulator of cell surface sialylation. *Science*, **284**, 1372–1376.

ELSEVIER

Brain & Development 29 (2007) 112–116

BRAIN & DEVELOPMENT
Official Journal of the Japanese Society of Child Neurology

www.elsevier.com/locate/braindev

Case Report

Familial reducing body myopathy

Maki Ohsawa [a,*], Teerin Liewluck [b], Katuhisa Ogata [c], Takahiro Iizuka [d], Yukiko Hayashi [b], Ikuya Nonaka [a], Masayuki Sasaki [a], Ichizo Nishino [b]

[a] *Department of Child Neurology, National Center Hospital for Mental, Nervous and Muscular Disorders, National Center of Neurology and Psychiatry (NCNP), Kodaira, Tokyo 187-8551, Japan*
[b] *Department of Neuromuscular Research, National Institute of Neuroscience, NCNP, Kodaira, Tokyo 187-8502, Japan*
[c] *Department of Neurology, National Center Hospital for Mental, Nervous and Muscular Disorders, NCNP, Kodaira, Tokyo 187-8551, Japan*
[d] *Department of Neurology, Kitasato University School of Medicine, Sagamihara, Kanagawa 228-8555, Japan*

Received 16 November 2005; received in revised form 22 June 2006; accepted 26 June 2006

Abstract

Reducing body myopathy (RBM) is a rare pathologically defined myopathy characterized by the presence of inclusion bodies which are abnormally stained by menadione–nitroblue–tetrazolium. The clinical symptoms vary widely as to the age of onset, disease progression and severity. Among the many reported patients, there have been only three families with this disorder, showing a manifold of clinicopathological features in each family. We report a fourth family with RBM affecting a boy and his mother. The proband (boy) began to have difficulty putting on his trousers at age 10 years and difficulty arising from a chair at 11 years. His spine was rigid. His mother, on the other hand, noticed foot-drop at the age 29, but the clinical course was rapidly progressive, and she was wheelchair-bound at 34 years. Both patients had generalized muscle weakness and atrophy and with mild CK elevation. Muscle pathology was characterized by the presence of atrophic fibers with reducing bodies in some areas. As these patients demonstrate, clinical symptoms in RBM are very variable, even within the same family. There are no specific clinical characteristics distinctive to RBM, thus further studies are necessary to characterize this disorder both clinically and pathologically.

Keywords: Reducing body myopathy; Familial; Mother and Son; Rapidly progressive

1. Introduction

Reducing body myopathy (RBM) is a group of heterogeneous disorders characterized pathologically by the presence of inclusion bodies that reduce nitroblue tetrazolium (NBT) in the absence of menadione as a substrate in the α-glycerophosphate dehydrogenase reaction. In 1972, Brooke and Neville initially described two unrelated girls with a severe congenital myopathy with reducing bodies [1]. The clinical spectrum of this disease is wide, showing different age of onset, course and severity of disease [2–10]. Although most of the cases have been sporadic, there have been three families with this disorder. Here, we report the fourth family with RBM and discuss the clinical and pathologic findings.

2. Patients and muscle pathology

2.1. Case history

The proband is an 11-year-old boy, the second of three children of a Japanese father and Filipino mother. Both his brothers were healthy except that the younger one had a history of Hirschsprung disease. Pregnancy

* Corresponding author. Tel.: +81 42 341 2711; fax: +81 42 344 6745.
E-mail address: mohsawa@ncnp.go.jp (M. Ohsawa).

0387-7604/$ - see front matter © 2006 Elsevier B.V. All rights reserved.
doi:10.1016/j.braindev.2006.06.010

and delivery were uneventful and psychomotor development was normal. Until 9 years of age, he could run faster than his classmates. At the age of 10 years and 5 months, he began to have difficulty putting on his trousers. One month after the onset, he developed foot-drop and began to fall frequently. Two months later, he had difficulty getting up from a sitting position. He could no longer run as fast as when he was 10 years old.

On physical examination, he had generalized muscle atrophy and weakness, especially around the shoulder, hip and anterior compartment of the lower legs. There was winging of the scapulae. Muscle weakness was slightly more marked on the left than the right. His spine was rigid on anteflexion and he had a lumbar lordosis. He was able to walk on his toes but not on his heels. Gowers' sign was positive. Deep tendon reflexes were diminished. Facial and extra-ocular muscles were normal. There were no fasciculations, calf muscle hypertrophy or pes cavus.

Cardiorespiratory functions were normal. The serum creatine kinase (CK) level was 495 IU/l (normal range 51–197 IU/l). Muscle CT scans revealed generalized volume loss, especially in the hamstrings, and areas of low density in the paraspinal muscles (Fig. 1). Needle electromyogram showed mixed neurogenic and myogenic patterns in biceps brachii and tibialis anterior muscles. Nerve conduction velocities of the median and tibialis posterior nerves were normal. No mutations were found in the SMN gene for spinal muscular atrophy; FSHD was ruled out by Southern blot.

The proband's mother is 35 years old. She developed foot-drop on the left at age 29 and became wheelchair-bound 5 years after the onset. Her father is Spanish and her mother is of Filipino and Chinese descent. Clinical examination revealed moderate generalized muscle atrophy and weakness. She was able to sit without support. She could raise her right arm up to the horizontal, but she was unable to raise her legs and left upper limb, against gravity. The spine was not rigid. Deep tendon reflexes were hypoactive. Facial and extra-ocular muscles were spared. The remainder of the physical examination was normal. Serum CK was slightly increased to 477 IU/l.

2.2. Muscle pathology

Muscle biopsy was performed on the left biceps brachii in the proband at age 11. His mother had two biopsies: left biceps brachii muscle and the left quadriceps femoris muscle at age 31. Biopsy specimens were frozen in isopentane cooled in liquid nitrogen. Serial 10 μm cryostat sections were stained with various histochemical methods. For electron microscopy, the muscle specimens were fixed in 2.5% glutaraldehyde in 0.1 M cacodylate buffer; ultrathin sections were double stained with uranyl acetate and lead citrate.

In the proband, there were clusters of atrophic fibers of 5–25 μm in diameter in a few fascicles (Fig. 2a–f), frequently with enlarged nuclei. Non-atrophic fibers showed moderate variation in fiber size ranging from 60–95 μm in diameter. Only a few fibers had internal nuclei. Endomysial fibrous tissue was increased in the atrophic fascicles. Adipose tissue was not increased. On modified Gomori trichrome (mGT), cytoplasmic bodies were seen in scattered fibers. There were no nemaline bodies, rimmed vacuoles or ragged-red fibers. On ATPase, there was mild fiber type grouping.

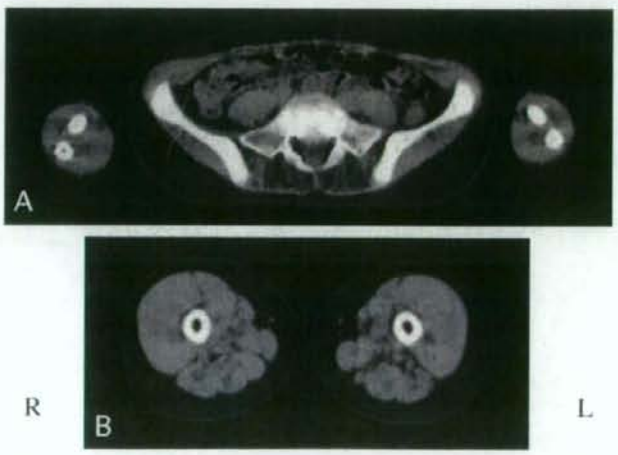

Fig. 1. Muscle computer tomography of the proband. The paraspinal muscles are almost totally replaced by fat tissue (A); the hamstring muscles are atrophic and exhibit moth-eaten appearance (B).

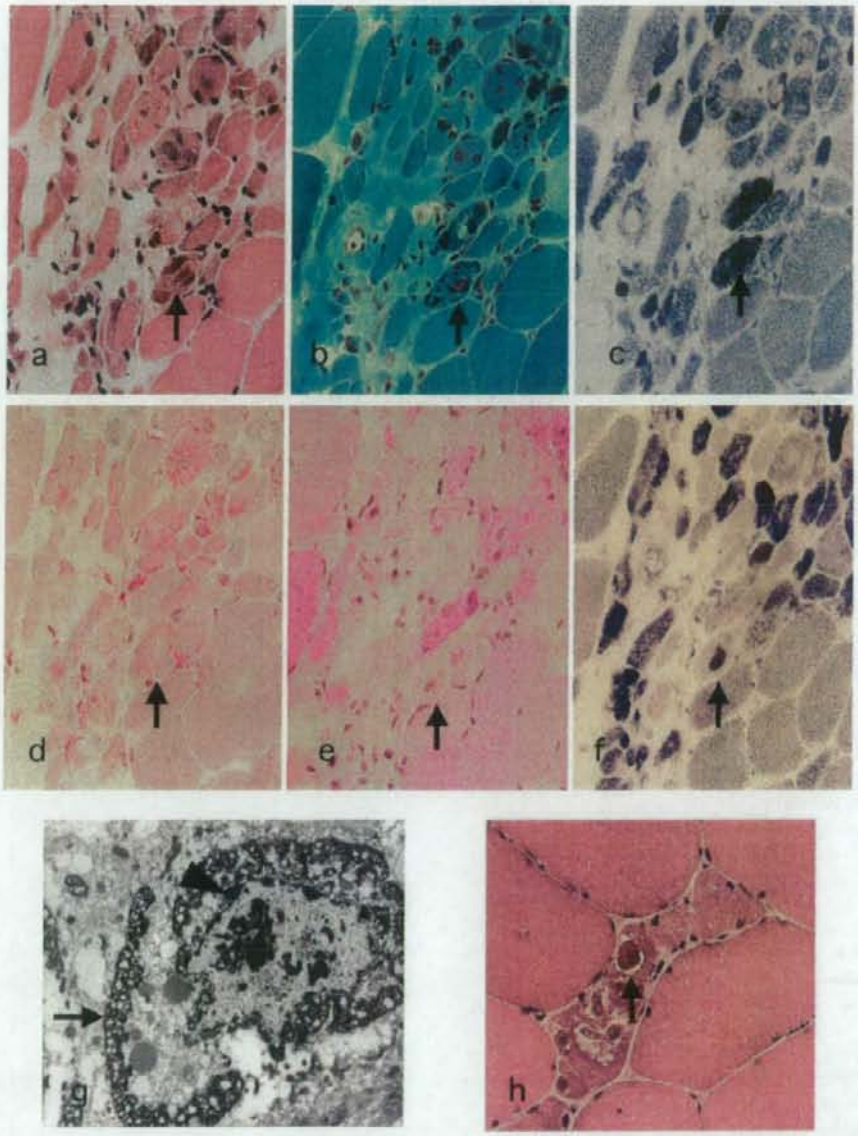

Fig. 2. Serial frozen sections (a–f) and an electron micrograph (g) from patient 1 and representative muscle pathology from patient 2 (h). In hematoxylin and eosin stain, atrophic fibers with reducing bodies are seen to be aggregated, (a). The reducing bodies are eosinophilic (a) and stained dark purple on modified Gomori trichrome (b), strongly reactive to NADH-TR (c), have increased enzymatic activity in acid phosphatase (d), and negative for periodic acid Schiff (PAS) staining suggesting that there is no glycogen component (e). They are strongly stained with MAG (f) showing "reducing activity" to nitroblue tetrazolium. Arrows in a–f indicate the same fiber with reducing bodies in serial sections. An electron micrograph of the reducing bodies (arrow) surrounding a degenerating nucleus (arrow head) suggesting a close relationship between nuclear change and inclusion body formation (g). In the proband's mother's muscle biopsy (h), there are fibers containing eosinophilic reducing bodies (arrow).

The most striking finding was the presence of reducing bodies in the atrophic fibers which were positively stained with both menadione-linked α-glycerophosphate dehydrogenase (MAG) and MAG without the substrate menadione. They were stained brilliant red with hematoxylin and eosin, dark purple with modified Gomori

trichrome, and dark blue with NADH-tetrazolium reductase.

On electron microscopy, these reducing bodies consisted of clusters of granular material with the same electron density as chromatin granules (Fig. 2g). They frequently encircled both normal-looking and degenerated myonuclei.

In the proband's mother, the overall pathological changes were similar although more fascicles were involved and contained very abundant reducing bodies (Fig. 2h). The inclusions were predominantly seen in type I fibers.

3. Discussion

Brooke and Neville were the first to describe two girls with congenital myopathy who had progressive and fatal courses [1] whose muscle biopsies were characterized by the presence of intracytoplasmic inclusion bodies. Since these inclusions reduce nitro-blue-tetrazolium (NBT) without a substrate in the α-glycerophosphate dehydrogenase reaction, the term "reducing body" was coined. Thereafter, many patients with reducing bodies in muscle biopsy have been reported as "reducing body myopathy" [2–10]. The onset of the disease varied from early childhood to adulthood, with different clinical symptoms; some had rapidly progressive and fatal course [1,6] and others showed a relatively benign course [2,5,9]. Initially, RBM was thought to be one of the congenital myopathies, although there is no characteristic clinical picture.

Although both our patients had proximal dominant muscle weakness and tibial muscle involvement other features varied: the onset of the disease was different, only the proband had rigid spine, and his mother's progression was quite rapid. Histopathologically, in both patients, some fascicles were preferentially affected. Inclusion bodies were seen mainly in the atrophic fibers.

There have been four families with RBM including the present family (Table 1) [2,7,10]. The modes of inheritance seem to be different from family to family: probable autosomal dominant or X-linked recessive inheritance in this family and in previous reports [7,8]. Hubner's family probably had an autosomal recessive inheritance. In familial RBM, many patients noticed their symptoms during school age, as in our proband; however, one patient developed weakness of the legs and hands after age 50 [10]. Rigid spine seems to be common in familial patients [7,10], but is not necessarily an initial sign and neither is it pathognomonic. Most patients had predominantly proximal muscle weakness and had no facial muscle involvement or pseudohypertrophy. Furthermore, serum CK was usually normal or only mildly elevated. However, there are no definite differences in clinical features between familial and spo-

Table 1
Previous reports of familial reducing body myopathy

Case	Sex	Onset age	Muscle weakness	Other symptoms	CK	Clinical course	Pathological findings	RB
Hubner et al. [2]	F	11	+	Respiratory insufficiency		27y: bed-ridden	Fibrosis	+
Sister	F	9	+	Respiratory insufficiency		15y: alive	Fibrosis	+
Reichmann et al. [7]	M	6	Proximal dominant	Rigid spine kyphosis	343	42y: wheelchair-bound, dead	Variation in fiber size fibrosis	+
Daughter	F	?	None	Rigid spine kyphosis				
Goebel et al. [10]	M	7	Proximal dominant	Rigid spine	174	8y: wheelchair-bound	Variation in fiber size	Many
Grand mother	F	50	Lower limbs dominant			70y: walk slowly	Small groups of atrophic fibers	+
Patient 1	M	10	Proximal dominant	Rigid spine	495	11y: unable to stand up without support	Focal atrophy	In atrophic fibers
Patient 2 (mother)	F	29	Proximal dominant		477	34y: wheelchair- bound	Focal atrophy	Mainly in atrophic fibers

CK: creatine kinase, RB: reducing body; ?: unknown.

radic patients. Pathologically, Goebel et al. [10] also reported that muscle fascicles with numerous inclusion bodies were adjacent to completely normal fascicles, and such focal degeneration seems to be a characteristic feature of this disorder [6]. It is still uncertain whether familial cases of RBM share a common pathogenetic mechanism with that in sporadic RBM.

Histopathologically there was fiber type grouping in our proband, suggesting a neurogenic process as well. Although needle electromyogram of the right tibialis anterior muscle showed a few giant spikes, careful clinical examination and peripheral nerve conduction studies showed no neurogenic changes. A prominent finding in RBM is that the atrophic fibers with reducing bodies are frequently aggregated in some fascicles, sparing the rest of the fascicle [6,10]. With disease progression, the changes extend diffusely and consequently fibrotic tissue proliferation ensues [6]. This selectivity of fascicular involvement may differ from muscle to muscle, reflecting different degrees and clinical variability.

The origin and significance of the reducing bodies remain unknown. Since these inclusions are usually present around and in the vicinity of myonuclei, association with nuclear changes appears possible, more so since these bodies have the same electron density as that of chromatin granules. By immunohistochemical staining, however, these bodies have no nuclear component.

Acknowledgements

We thank Ms Fumie Uematsu for taking electron micrographs on muscle biopsies. The authors thank Dr. May Christine V. Malicdan for her critical comments on the manuscript. This work is supported in part by the "Research on Health Sciences focusing on Drug Innovation" and the "Research on Psychiatric and Neurological Diseases and Mental Health" from the Japanese Health Sciences Foundation; in part by the "Grant-in-Aid for Scientific Research" from the Japan Society for the Promotion of Science; and in part by the "Research Grant (17A-10) for Nervous and Mental Disorders" from the Ministry of Health, Labour and Welfare.

References

[1] Brooke MH, Neville HE. Reducing body myopathy. Neurology 1972;22:829–40.
[2] Hübner G, Pongratz D. Reducing body myopathy – ultrastructure and classification (author's transl). Virchows Arch A Pathol Anat Histol 1981;392:97–104.
[3] Oh SJ, Meyers GJ, Wilson Jr ER, Alexander CB. A benign form of reducing body myopathy. Muscle Nerve 1983;6:278–82.
[4] Carpenter S, Karpati G, Holland P. New observations in reducing body myopathy. Neurology 1985;35:818–27.
[5] Bertini E, Salviati G, Apollo F, Ricci E, Servidei S, Broccolini A, et al. Reducing body myopathy and desmin storage in skeletal muscle: morphological and biochemical findings. Acta Neuropathol (Berl) 1994;87:106–12.
[6] Kiyomoto BH, Murakami N, Kobayashi Y, Nihei K, Tanaka T, Takeshita K, et al. Fatal reducing body myopathy. Ultrastructural and immunohistochemical observations. J Neurol Sci 1995;128:58–65.
[7] Reichmann H, Goebel HH, Schneider C, Toyka KV. Familial mixed congenital myopathy with rigid spine phenotype. Muscle Nerve 1997;20:411–7.
[8] Goebel HH. Congenital myopathies with inclusion bodies : a brief review. Neuromuscul Disord 1998;8:162–8.
[9] Figarella-Branger D, Putzu GA, Bouvier-Labit C, Pouget J, Chateau D, Fardeau M, et al. Adult onset reducing body myopathy. Neuromuscul Disord 1999;9:580–6.
[10] Goebel HH, Halbig LE, Goldfarb L, Schober R, Albani M, Neuen-Jacob E, et al. Reducing body myopathy with cytoplasmic bodies and rigid spine syndrome : a mixed congenital myopathy. Neuropediatrics 2001;32:196–205.